

Synthesis of hydroxyapatite with adsorbed and intracrystalline biomolecules

By

Julien Guiu

Ingénieur Diplômé de l'Ecole Centrale Paris (1997)
Paris, France

Submitted to the Department of Materials Science and Engineering
In Partial Fulfillment of the Requirements for the Degree of

Master of Science in Materials Science and Engineering

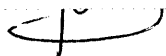
at the

Massachusetts Institute of Technology

June 1999

© 1999 Massachusetts Institute of Technology
All rights reserved

Signature of Author



.....
Department of Materials Science and Engineering
May 7, 1999

Certified by

.....
Sandra L. Burkett
John Chipman Assistant Professor of Materials Chemistry
Department of Materials Science and Engineering
Thesis Supervisor

Accepted by

.....
Linn W. Hobbs
John F. Elliot Professor of Materials
Chairman, Departmental Committee on Graduate Students



Room 14-0551
77 Massachusetts Avenue
Cambridge, MA 02139
Ph: 617.253.2800
Email: docs@mit.edu
<http://libraries.mit.edu/docs>

DISCLAIMER OF QUALITY

Due to the condition of the original material, there are unavoidable flaws in this reproduction. We have made every effort possible to provide you with the best copy available. If you are dissatisfied with this product and find it unusable, please contact Document Services as soon as possible.

Thank you.

The images contained in this document are of the best quality available.

Synthesis of hydroxyapatite with adsorbed and intracrystalline biomolecules

By

Julien Guiu

Submitted to the Department of Materials Science and Engineering on May 7, 1999
In Partial Fulfillment of the Requirements for the Degree of
Master of Science in Materials Science and Engineering

Abstract:

A hydrothermal synthesis of hydroxyapatite (HAp) was developed to allow the preparation of HAp at temperatures between 120 °C and 220 °C. The purity and the microstructure of the HAp samples were investigated using X-ray powder diffraction, Fourier-transform infrared spectroscopy and Transmission electron microscopy. The properties of the products were found to be highly dependent on the reaction temperature. At higher temperatures higher temperatures, higher-purity samples with needle-like crystallites were formed. The synthesis procedure at 170 °C was used for incorporation of amino acids in the HAp inorganic framework. The influence of five representative amino acids with five different types of side chains (R groups) on the reaction product was investigated. It was found that, under the reaction conditions, amino acids with a negative charge and a polar side chain had the greatest influence on the crystallization process. Phenylalanine, which does not have a polar side chain, also appears to strongly interact with the inorganic network. For incorporation of whole proteins, such as lysozyme, an alternative room temperature synthesis procedure was developed. This method involves trapping lysozyme in the HAp network during pH-controlled precipitation. Lysozyme was labeled with a fluorescent probe (fluorescein isothiocyanate or FITC) in order to facilitate detection of intracrystalline proteins by spectrofluorimetry. The products containing intracrystalline protein inclusions were contrasted with samples containing surface-adsorbed proteins.

Thesis supervisor: Dr. Sandra L. Burkett

CONTENTS:

LIST OF FIGURES:	5
LIST OF TABLES:	7
ACKNOWLEDGMENTS:.....	8
II- BIOMINERALIZATION:.....	12
II-1 THE MINERALS:	12
II-2 BIOMINERALIZATION PROCESSES:.....	14
II-2-a Spatial delineation:.....	14
II-2-b Influence of additives in biomineralization:	14
II-2-c Control over nucleation:.....	15
II-3 EXAMPLES OF BIOMINERALIZATION:	15
II-3-a Ferritin [4]:	15
II-3-b Calcite-Aragonite deposition in mollusk shells [1,2, 4-6,7]:.....	16
III- SYNTHESIS OF HYDROXYAPATITE:.....	21
III-1 STRUCTURE AND COMPOSITION OF APATITE MINERALS:.....	21
III-2 MATERIALS AND METHODS	23
III-2-a Materials:	23
III-2-b Preparation of hydroxyapatite particles:	23
III-2 ANALYSES:.....	25
III-2-a X-ray diffraction:.....	25
III-2-b Infrared spectrometry (FTIR):.....	28
III-2-c TEM micrography:	31
III-2-d Determination of surface area:	31
III-3 DISCUSSION:.....	33
IV- INCORPORATION OF AMINO-ACIDS:	34
IV-1 MATERIALS AND METHODS:	34
IV-2 RESULTS:	35
IV-2-a Alanine:	35
IV-2-b Phenylalanine:.....	36
IV-2-c Threonine:.....	41
IV-2-d Arginine:.....	46
IV-2-e Aspartic acid:.....	49
IV-3 DISCUSSION:	54
V- PROTEIN ENTRAPMENT IN HYDROXYAPATITE:.....	59
V-1 PRECIPITATION OF HAP WITH PROTEIN ENTRAPPED	59
V-1-a Materials.....	59
V-1-b Preparation of the protein solution.....	60
V-1-c Precipitation of HAp in the presence of protein:	61
V-1-d Adsorption of FITC-lysozyme on precipitated HAp:.....	61
V-1-e Dissolution of HAp in EDTA buffer:	62
V-2 RESULTS:.....	62
V-2-a Fluorescence Emission of FITC-lysozyme conjugates:.....	62
V-2-b X-ray diffraction:	67
V-2-c Infrared spectrometry:	67
V-3 DISCUSSION:.....	68

VI- ADSORPTION OF LYSOZYME ON HAP:	72
VI-1 INTERACTIONS WITH HYDROXYAPATITE [18-21]:.....	72
<i>VI-1-a Classification of proteins:</i>	73
<i>VI-1-b Characteristics of adsorption/elution behavior of basic proteins:</i>	73
VI-2 MATERIALS AND METHODS:	74
<i>VI-2-a Materials:</i>	74
<i>VI-2-b Methods:</i>	74
VI-3 RESULTS AND DISCUSSION:	77
<i>VI-3-a Adsorption isotherms:</i>	77
<i>VI-3-b Cooperativity and Hill equation:</i>	82
VI-4: DISCUSSION	84
VII- CONCLUSION:	87
BIBLIOGRAPHY:	89

List of Figures:

<u>Figure II-1:</u>	Schematic model of the organic matrix in a mollusk shell nacreous layer [2].	18
<u>Figure II-2:</u>	Possible modes of molecular complementarity between Ca atoms in the aragonite ab face and aspartic acid residues organized in the sequence Asp-X-Asp (X=neutral residue such as alanine) along the β -sheet matrix interface. [6].	19
<u>Figure III-1:</u>	XRD spectra for HAp 130, 170, 220 °C, and precipitated.	27
<u>Figure III-2:</u>	Time dependence of the hydrothermal synthesis at 170 °C.	29
<u>Figure III-3:</u>	FTIR spectra of HAp 130 °C, 170 °C, 220 °C and precipitated	30
<u>Figure III-4:</u>	HAp 130 °C	32
<u>Figure III-5:</u>	HAp 170 °C	32
<u>Figure III-6:</u>	HAp 220 °C	32
<u>Figure III-7:</u>	precipitated HAp	32
<u>Figure IV-1:</u>	pH-dependant ionization states of amino acids.	35
<u>Figure IV-2:</u>	Influence of alanine on the XRD spectrum of HAp at 170 °C.	37
<u>Figure IV-3:</u>	Influence of alanine on the FTIR spectrum of HAp at 170 °C.	37
<u>Figure IV-4:</u>	HAp 170 °C.	38
<u>Figure IV-5:</u>	HAp 170 °C with alanine.	38
<u>Figure IV-6:</u>	Influence of phenylalanine on the XRD spectrum of HAp at 170 °C.	40
<u>Figure IV-7:</u>	Influence of phenylalanine on the FTIR spectrum of HAp at 170 °C.	40
<u>Figure IV-8:</u>	Influence of the adsorption of phenylalanine on the FTIR spectrum of HAp at 170 °C	42
<u>Figure IV-9:</u>	HAp 170 °C.	43
<u>Figure IV-10:</u>	HAp 170 °C with phenylalanine.	43
<u>Figure IV-10:</u>	Influence of threonine on the XRD spectrum of HAp at 170 °C.	45
<u>Figure IV-11:</u>	Influence of threonine on the FTIR spectrum of HAp at 170 °C.	45
<u>Figure IV-12:</u>	Influence of the adsorption of threonine on the FTIR spectrum of HAp at 170 °C.	47
<u>Figure IV-13:</u>	HAp 170 °C.	48
<u>Figure IV-14:</u>	HAp 170 °C with threonine.	48
<u>Figure IV-15:</u>	Influence of arginine on the XRD spectrum of HAp at 170 °C.	50
<u>Figure IV-16:</u>	Influence of arginine on the FTIR spectrum of HAp at 170 °C.	50
<u>Figure IV-17:</u>	HAp 170 °C.	51
<u>Figure IV-18:</u>	HAp 170 °C with arginine.	51
<u>Figure IV-19:</u>	Influence of aspartic acid on the XRD spectrum of HAp at 170 °C.	53
<u>Figure IV-20:</u>	Influence of aspartic acid on the FTIR spectrum of HAp at 170 °C.	53
<u>Figure IV-21:</u>	Influence of the adsorption of aspartic acid on the FTIR spectrum of HAp at 170 °C.	55
<u>Figure IV-22:</u>	HAp 170 °C.	56
<u>Figure IV-23:</u>	HAp 170 °C with aspartic acid.	56
<u>Figure V-1:</u>	FITC conjugate with ϵ -amino group of a lysine residue in a protein.	60
<u>Figure V-2:</u>	pH-dependent FITC-lysozyme fluorescence intensity normalized by the fluorescence intensity at pH 9.2 at $\lambda=525$ nm.	64
<u>Figure V-3:</u>	Quenching of FITC fluorescence by methyl viologen at $\lambda=525$ nm.	65
<u>Figure V-4:</u>	Determination of the Stern-Volmer constant at $\lambda=525$ nm.	66
<u>Figure V-5:</u>	Fluorescence emission of HAp precipitated with FITC lysozyme entrapped and adsorbed after treatment by 1% hypochloride.	69
<u>Figure V-6:</u>	UV-visible absorption spectrum of HAp/FITC-lysozyme precipitate; treated with 1% hypochloride then dissolved in EDTA buffer	69
<u>Figure V-8:</u>	Influence of lysozyme on the XRD spectrum of HAp precipitated.	70
<u>Figure V-9:</u>	Influence of lysozyme on the FTIR spectrum of HAp precipitated.	70
<u>Figure V-10:</u>	Precipitated HAp.	71
<u>Figure V-11:</u>	Precipitated HAp with FITC-lysozyme.	71
<u>Figure VI-1:</u>	Schematic representation of side-on and end-on adsorption	75

<u>Figure VI-2:</u>	Adsorption onto Hap of lysozyme.....	78
<u>Figure VI-3:</u>	Adsorption isotherm of lysozyme (Γ as a function of concentration).	78
<u>Figure VI-4:</u>	Surface coverage for lysozyme adsorption on HAp.	81
<u>Figure VI-5:</u>	Surface coverage of the adsorption of lysozyme on HAp precipitated.....	81
<u>Figure VI-6:</u>	Schematic possible change of conformation due to the lateral interaction between the proteins on the surface and the interactions between protein and adsorbent.	82
<u>Figure VI-7:</u>	Hill plots for adsorption of lysozyme onto hydrothermally synthesized HAp samples.....	85
<u>Figure VI-8:</u>	Hill plot for adsorption of lysozyme onto precipitated HAp	85

List of Tables:

<u>Table III-1:</u>	Apatite crystallographic data.	21
<u>Table III-2:</u>	Crystallographic parameters for hydroxyapatite.....	24
<u>Table III-2:</u>	Influence of the synthesis temperature on sample surface area.	30
<u>Table VI-1:</u>	Properties of lysozyme.	75
<u>Table VI-2:</u>	High concentration adsorption behavior of HAp.....	76
<u>Table VI-3:</u>	Calculated Hill coefficients.	83

Acknowledgments:

I would like to acknowledge, first and foremost, my advisor Sandra L. Burkett for giving me the opportunity to participate in this project, for strongly supporting me in my endeavors, and for providing me with challenge and inspiration. Her advice and knowledge has helped me improve my understanding of the topics involved.

I am deeply grateful for all the help provided by Michael Read from my research group for his availability and his advice. His help was invaluable and I have no doubt that his Ph.D. work will be terrific.

I would also like to thank Joe Adario (XRD), Lenny Rigione (SEN), John Centerino, Mike Frongillo (TEM), Dr. G. Reed (TEM), Tim Mc Clure, Elizabeth Shaw (XPS) for their time and their expertise of the different equipment I have been using.

I am also grateful for the kindness from the members of Cima research group.

Last but not least, I would like to thank Skander Oueslati, Renaud Bruyeron and especially Eric Marandon for their friendship and their help in keeping me motivated.

I would also like to thank to French soccer team for, at last, having won the World Cup. That was definitely one of the greatest moments of those two years.

I- Introduction:

Bioceramics comprise a rapidly advancing area of technology and play integral roles in devices used in biotechnology and medicine. Much effort is spent tailoring the properties of these materials to satisfy critical performance criteria under operating conditions. The parallel investigations of natural materials, particularly products of biomineralization processes that occur in many microorganisms, animals, and plants have underlined the importance of organic matrices in the deposition of mineral and mineralized phases. Organic molecules and macromolecules appear influence strongly the crystallization of biogenic inorganic minerals by providing stereospecific control of nucleation, crystal orientation, or polymorph selectivity. Morse et al. have demonstrated in vivo and in vitro that both insoluble protein matrices and soluble intracrystalline polyanionic proteins have a great influence in the regulation of nucleation, growth, morphology, aggregation, and phase selectivity (between aragonite and calcite polymorphs) of calcium carbonate (CaCO_3) in the biosynthesis of mollusk shells ([1]).

The goal of this work is to study interactions between organic molecules and hydroxyapatite (HAp). Hydroxyapatite ($\text{Ca}_{10}(\text{PO}_4)_6(\text{OH})_2$) is the mineral component of bone. It is precipitated in a complex matrix of collagen, glycoproteins and proteoglycans and is responsible for the mechanical stiffness of bones. A lot of work is being done on this material because of its biocompatibility, which makes it a good candidate for implant coatings or drug delivery devices.

The first objective of this thesis was to design a low temperature synthesis of hydroxyapatite that would allow to incorporation of biomolecules. Samples were characterized by X-ray powder diffraction (XRD) and by Fourier transform infrared

spectroscopy (FTIR) to confirm the composition of the sample and to clarify the influence of reaction temperature on crystallinity and the carbonate content of the samples. TEM analysis allowed a microscopic description of the HAp particles.

Amino acids are the basic components of proteins and can be classified in five categories by the chemical properties of their side chains (R): nonpolar, aliphatic R groups; aromatic R groups; cationic R groups; anionic R groups; polar, uncharged R groups. The interaction of a representative amino acid, from each of the five different groups, during synthesis of the inorganic material was studied. XRD, FTIR and TEM observations suggested that several amino acids strongly interact with HAp during synthesis such that intracrystalline inclusions and/or formation of different calcium phosphate phases were formed.

Although this synthesis procedure was designed for incorporation of small organic molecules, the temperature was still too high to permit use of proteins in the crystallization process. Therefore, a synthesis procedure involving precipitation at room temperature was developed such that intracrystalline inclusions of lysozyme in HAp could be introduced. Lysozyme was labeled with a fluorescent probe (fluorescein isothiocyanate or FITC) in order to monitor more easily the intracrystalline molecules with spectrofluorimetry.

Finally, interactions between HAp surfaces and lysozyme were investigated by experiments involving adsorption of lysozyme from buffer solution. UV visible spectrometry was used to quantify the amounts of protein adsorbed on the different samples as a function of synthesis temperature, carbonate content, and surface areas.

The first part will underline the main principles of biomineralization and the ideas behind this work. Then the two different syntheses of HAp were described and the precipitates characterized. The next two chapters present the influence of amino acids on the crystallization of Hap and the entrapment of lysozyme. The results of lysozyme adsorption on HAp surfaces are presented in chapter 5.

II- Biomineralization:

Biomineralization is the process by which organisms including microorganisms, animals, and plants, convert inorganic ions in aqueous solution into solid mineral phases. Mineral deposition in biological systems can be beneficial to an organism in a structural role (e.g. formation of bones, teeth, and shell material) or in a metabolic role (e.g. accumulation and storage of essential elements such as calcium and phosphorous). These transformations are regulated by cellular activities that make possible the physicochemical changes necessary for mineral formation and crystal growth.

II-1 The minerals:

A wide variety of elements are found in biologically mineralized systems including common elements such as H, C, O, Mg, Si, P, S, Ca, Mn and Fe as well as rarer elements such as Au, Pb, Sr, Ba or Zn. Almost 60 different biogenic minerals have been discovered (see Table 1) and more than 60% of them exist as hydrates or hydroxides.

The major mineralized tissues such as bones and teeth or shells are composed of calcium phosphate or calcium carbonate minerals, respectively, in combination with a complex organic macromolecular matrix of proteins, polysaccharides, and lipids. The prevalence of calcium biominerals, which are thermodynamically very stable, can be explained by the high concentrations of Ca^{2+} in extracellular fluids and the low solubility product of their carbonates (CO_3^-), phosphates (PO_4^{3-} , 25% of known biogenic phase), sulfates (SO_4^{2-}), pyrophosphates ($\text{P}_2\text{O}_7^{4-}$) and oxalates ($\text{C}_2\text{O}_4^{2-}$). This strong thermodynamic driving force provides very effective means to regulate ionic concentrations in biological fluids for both homeostasis and detoxification.

MINERAL PHASE	FORMULA	ORGANISM	FUNCTION	
<i>Calcium carbonate</i>	Calcite	CaCO ₃	Algae, Mollusks	Exoskeletons
			Crustaceans	Eye lenses
			Sea Urchins	Spicules
	Aragonite	CaCO ₃	Mollusks	Exoskeletons (nacre)
			Cuttlefish	Buoyancy device
	Vaterite	CaCO ₃	Crustaceans	Gravity perception
Amorphous	CaCO ₃ •nH ₂ O	Plants	Calcium store	
<i>Calcium phosphate</i>	Hydroxyapatite	Ca ₁₀ (PO ₄) ₆ (OH) ₂	Vertebrates	Endoskeletons, Teeth, Calcium store
	Octacalcium phosphate	Ca ₈ H ₂ (PO ₄) ₆	Vertebrates	Precursor to bone?
	Amorphous	Ca _x (PO ₄) _y (OH) _z	Crustaceans	Cuticle
<i>Calcium oxalate</i>	Whewellite	CaC ₂ O ₄ •H ₂ O	Plants	Calcium store
	Weddelite	CaC ₂ O ₄ .2H ₂ O	Plants	Calcium store
<i>Group IIA Metal sulfates</i>	Gypsum	CaSO ₄	Jellyfish larvae	Gravity device
	Barite	BaSO ₄	Algae	Gravity device
	Celestite	SrSO ₄	Acantharia	Cellular support
<i>Silicon dioxide</i>	Silica (amorphous)	SiO ₂ .nH ₂ O	Diatoms	Exoskeletons
			Plants	Hairs, spore, coats
<i>Iron Oxide</i>	Magnetite	Fe ₃ O ₄	Bacteria	Magnetotaxis
			Chitons	Teeth
	Goethite	α-FeOOH	Limpets	Teeth
	Lepidocrocite	γ-FeOOH	Chitons	Teeth
Ferrihydrite	5Fe ₂ O ₃ •9H ₂ O	Animals, Plants	Iron storage proteins (ferritin)	
<i>Other minerals</i>	Gold	Au	Bacteria	Unknown
	Ice	H ₂ O	Bacteria	Unknown

TableII-1: Some common biologically-formed minerals.

II-2 Biomineralization processes:

Although a wide variety of organisms form carbonate- and phosphate-containing biogenic minerals, in most cases these biominerals are formed in the presence of acidic, negatively charged glycoproteins and proteoglycan matrices. These proteins are rich in acidic amino acids such as aspartic and glutamic acids and, in many cases, phosphorylated serine and threonine residues. It appears that many organisms have developed common strategies for the regulation mineral formation.

II-2-a Spatial delineation:

A distinctive feature of biologically-controlled mineralization is compartmentalization, or the enclosure of the reaction site by lipid bilayers or sheets of polymerized water-insoluble macromolecules, either in the cell membrane or outside the cell, which will prevent the diffusion of ions. Spatial delineation as a mean for controlling mineralization, facilitates the establishment of a locally supersaturated solution, through the use of ion pumps for example, from which mineral precipitation occurs.

II-2-b Influence of additives in biomineralization:

The ability of soluble additives to influence crystal nucleation and growth in synthetic systems is a well-known phenomenon [2], and is the basis for many industrial processes. Interactions between those species and the surfaces of the growing crystals depend on the chemistry and geometry of the crystal surfaces and of the additives. Subtle changes such as the position of a hydrogen bond in molecules of chiral additives, for example, can result in large alterations in the morphology of the crystals [3]. An additive

can influence the crystal structure if the geometric and chemical complementarity is such that the additives interact selectively with certain crystal faces. These interactions retard growth of specific faces. Alternatively, the additives can interact with the mineral nuclei and inhibit the nucleation of some phases while inducing others to form.

II-2-c Control over nucleation:

Organic matrices such as vesicle bilayers or acidic glycoproteins and proteoglycans located on the surfaces of organic framework matrices, can serve as sites of controlled heterogeneous nucleation. Due to the technical difficulties involved in studying structures of the length scale of critical nuclei (\cong a few nm), most of the information regarding nucleation of biominerals has been acquired through observation of spatial relationships between the resulting crystals and the nucleation matrix. The relative orientations of the macromolecules can be inferred from the crystallographic orientation of the mineralized crystals.

II-3 Examples of biomineralization:

Examples of biomineralization are presented to illustrate key features of mineralization strategies that provide the inspiration for the synthetic approaches and goals addressed in this thesis.

II-3-a Ferritin [4]:

A classic example of compartmentalization and nucleation control occurs in ferritin. This iron storage protein consists of a spherical protein shell that surrounds an inorganic core of iron oxide, in the form of the mineral, ferrihydrite. The micelle is

constructed from the self-assembly of 24 polypeptide subunits arranged in cubic symmetry such that molecular channels penetrate the shell. The metal-binding, oxidation sites which are composed of three carboxylate ligands that stabilize incipient iron (III) nuclei by charge and polar interactions, are present in the H-chain but not in the L-chain. This site is close to the inner surface of the protein shell such that iron (III) species formed at the ferroxidase center migrate into the cavity. The 8 nm diameter of the internal cavity sets an upper limit to the size of the mineral core. The specific molecular processes (oxidation and site-directed nucleation) that control mineralization are confined to this nanospace and they compete successfully against non-specific reactions occurring in the external medium. Functionally, this is very important because it prevents precipitation of iron oxide outside the protein shell (rust is very toxic) and thus iron storage and transport are closely regulated by ferritin biomineralization within the organism.

II-3-b Calcite-Aragonite deposition in mollusk shells [1,2, 4-6,7]:

Many mineralizing organisms deposit either calcite or aragonite, which are two closely-related polymorphs of calcium carbonate; calcite is the thermodynamically stable phase under ambient conditions. Although the presence of magnesium ions can favor the formation of aragonite, the organic matrix plays a major role in controlling the polymorph selectivity and spatial distribution.

In the nacreous layer of mollusk shells the orientations of the crystallographic axes of aragonite are known with respect to the chitin and silk-fibroinlike β -sheet proteins that constitute the matrix framework. Chemical studies on *Nautilus Pompeus* (a cephalopod) and *Mercenaria mercenaria* (a clam) indicate that matrix proteins are

composed of two structural units: (1) a polypeptide with a strong affinity to Ca^{2+} ions which appears to act as a structurally-organized nucleation site by binding Ca^{2+} ions in a configuration that resembles to the a-b plane of aragonite, and (2) a high molecular weight protein which is arranged in the form of sheets and layers and which has no affinity for calcium (figure 1). Attachment of the acidic macromolecules on the matrix framework apparently activates the mineralizing substrate and calcium carbonate crystals are laid down in epitaxial order. Crystal growth terminates upon secretion of a newly formed layer of macromolecules [2]. The result is a mosaic of aragonite crystals with the c-axes aligned perpendicular to the matrix surface but with different crystallographic orientations of the a- and b-axes.

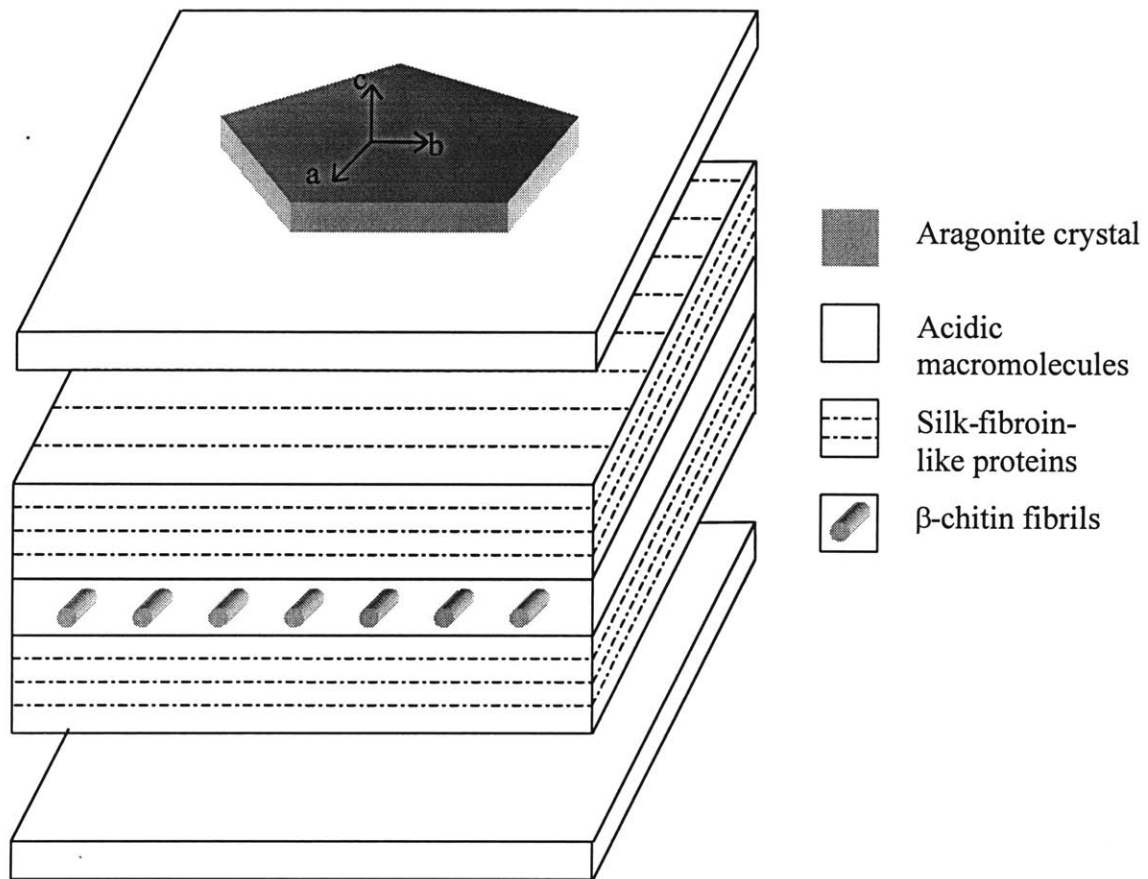


Figure II-1: Schematic model of the organic matrix in a mollusk shell nacreous layer [2].

Comparison of the Ca^{2+} - Ca^{2+} distances in the a-b plane of aragonite and the matrix periodicity shows a close matching for the a-axis (0.496 nm and 0.470 nm, respectively) whereas a greater difference appears for the b-axis (0.797 nm and 0.690 nm, respectively). Since binding of individual Ca^{2+} to carboxylate groups is generally cooperative, involving at least two or three carboxylic acid groups [8], an amino-acid sequence of Asp-X-Asp (X being a neutral residue) along the β -sheet framework has been suggested to provide an optimum binding surface for calcium ions and a favorable nucleation configuration for calcium carbonate [9] (Figure II-2).

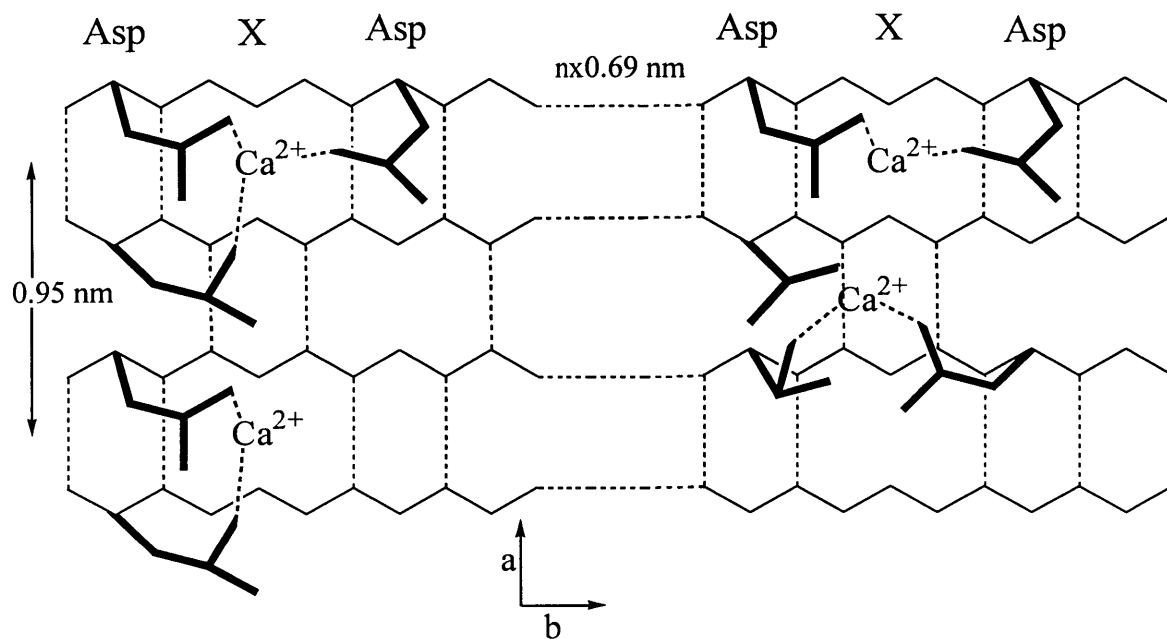


Figure II-2: Possible modes of molecular complementarity between Ca atoms in the aragonite ab face and aspartic acid residues organized in the sequence Asp-X-Asp (X=neutral residue such as alanine) along the β -sheet matrix interface. [6].

Sequences of this type are common in proteins found after solubilization by EDTA of both aragonite and calcite layers of mollusk shells [10], [11]. Polyanionic proteins that appear to provide stereospecific control of nucleation, crystal orientation, polymorph phase, and switching back and forth between phases, beyond the first layer determined by the nucleating sheet, are found within the aragonite and calcite crystal. These additional proteins are entrapped in the mineral network, and they can be isolated only by dissolving the inorganic network. In *in vitro* experiments, addition of some of these soluble shell proteins is sufficient to promote polymorph selectivity calcium carbonate structures. For example, crystals grown in the absence of soluble protein exhibit the characteristic rhomboedral morphology of calcite whereas crystals grown with

polyanionic proteins isolated from an aragonite region a red abalone shell induced the formation of aragonite needles [1].

These latter experiments underline the importance of intracrystalline protein inclusions in the biomineralization process. The question arises as how organic materials can be entrapped in the inorganic network and through what types of interactions this entrapment occurs. The observation that protein inclusions in inorganic crystals can occur in biological systems provide inspiration for the development of synthetic composite materials that consist of organic molecules or proteins entrapped as intracrystalline inclusions within inorganic matrices. An interesting application would be the realization of a drug delivery system consisting of a resorbable biocompatible mineral with drugs entrapped in the inorganic framework. The composite would be implanted in the body and would regularly release the medication. The high biocompatibility of hydroxyapatite makes it a good candidate for this application. Therefore, the interactions of proteins and amino acids with hydroxyapatite are studied in this thesis to investigate the suitability of hydroxyapatite for this utilization.

III- Synthesis of hydroxyapatite:

III-1 Structure and composition of apatite minerals:

The similarities between the XRD spectra of enamel, dentin, bone and those of non-biogenic mineral apatites, coupled with chemical analyses that show calcium and phosphate to be the primary components of these materials has led to the conclusion that bone and teeth are mainly constituted of calcium hydroxyapatite (HAp), with the idealized composition as $\text{Ca}_{10}(\text{PO}_4)_6(\text{OH})_2$. However, to date, the exact structure of biological apatites remains unknown.

“Apatite” describes a family of compounds that have similar crystal structures but a wide range of compositions. Apatites belong to the hexagonal crystallographic space group $\text{P6}_3/\text{m}$. The unit cell contains 10 Ca^{2+} ions, 6 PO_4^{3-} groups and 2 OH^- groups closely packed together. The ten calcium ions are divided between Ca(I) or Ca (II) sites: four calcium ions occupy Ca(I) positions at levels ($z=0$) and two at $z=0.5$; six atoms occupy Ca(II) positions, with three located at $z=0.25$, and the other three at $z=0.75$, surrounding the OH^- ions located at the corners of the unit cell. The six PO_4^{3-} tetrahedra are arranged in sets of three at levels $z=0.25$ and $z=0.75$. The network of PO_4^{3-} groups provide the skeletal framework of the apatite and gives the apatite structure its stability. The atomic arrangements of fluoroapatite (F instead of OH) and of chloroapatite (Cl instead of OH) are similar to that in HAp with respect to the Ca^{2+} and PO_4^{3-} atoms but differ in respective positions of OH^- , F^- and Cl^- , along the c-axis. These substitutions for OH^- give rise to changes in the lattice parameters, depending on the relative size of the substituting group (Table III-1).

	Fluoroapatite	Hydroxyapatite HAp	Chloroapatite
Ionic radii of X (=F, OH, Cl)	1.36 Å	1.53 Å	1.81 Å
Ca-X distance in apatite	2.29 Å	2.89 Å	2.8 Å
Lattice parameters (error: 0.005 nm)			
a-axis	9.375 nm	9.422 nm	9.647 nm
c-axis	6.880 nm	6.882 nm	6.771 nm
Unit-cell volume (Å ³)	523	530	545

Table III-1: Apatite crystallographic data.

Non-stoichiometry of biological apatites is due to the presence of minor components such as Mg²⁺, Na⁺, K⁺ (for Ca²⁺), CO₃²⁻ (for PO₄³⁻), Cl⁻ or F⁻ (for OH⁻). Synthetic carbonate apatites show two types of CO₃²⁻ substitutions: type A substitutions (CO₃²⁻ for OH⁻) occur in samples prepared at high temperature and dry conditions [12], whereas type B substitutions (CO₃²⁻ for PO₄³⁻) arise in samples prepared in aqueous media at lower temperatures (25 °C to 100 °C), either by precipitation or hydrolysis methods [13, 14]. Type A substituted apatites have IR vibrational modes in the carbonate region at 1528 cm⁻¹, 1465 cm⁻¹ and 878 cm⁻¹, whereas the carbonate peaks for type B samples occur at 1540 cm⁻¹, 1455 cm⁻¹, 1414 cm⁻¹, and 872 cm⁻¹ [13]. The effect of CO₃²⁻ substitution on the lattice parameters depends on the substitution: type A substitutions cause expansion of the a-axis and contraction of the c-axis whereas type B substitutions cause contraction of both the a-axis and the c-axis.

III-2 Materials and methods

III-2-a Materials:

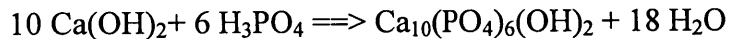
The following materials were used as obtained from the manufacturer: Ca(OH)₂ (Aldrich, USA), 0.6 N phosphoric acid (EM Science), 0.1 N HCl (Aldrich, USA), KOH (Mallinckrodt Chemical), 1000 ml Pyrex beaker, high purity deionized water was used (US Filter, Purelab Plus UV/UF). The syntheses were conducted in Teflon™-lined stainless steel Acid Digestion Bombs (23 ml; Parr Instrument Company).

III-2-b Preparation of hydroxyapatite particles:

The first objective was to develop a simple and reliable synthesis of hydroxyapatite (HAp) that does not require very high temperatures and pressure, since the ultimate goal was to incorporate organic components such as amino-acids, which decompose at temperatures above 200 °C. Incorporation of proteins required a different procedure able to produce HAp at very mild temperature to avoid denaturation and decomposition of the protein.

III-2-b-i Hydrothermal synthesis:

Suspensions of HAp were prepared according to the following reaction:



The synthesis was performed at temperatures ranging from 130 to 220°C. In each case, the reactants were weighed carefully such that the Ca/P ratio was maintained at the

stoichiometric value for HAp (Ca/P=1.67) in order to avoid formation of other calcium phosphate phases.

In a typical synthesis, 0.01 mole of $\text{Ca}(\text{OH})_2$ (0.741 g) was added to 10 ml of H_3PO_4 (0.6 M) in a 23 ml Teflon™ cup, and the solution was stirred for 20 minutes until a basic pH (approx. pH 12) was reached. The Teflon™ cup was sealed in a digestion bomb and placed in the oven at the desired temperature for 24 hours.

The precipitate was vacuum filtered, washed with deionized water, and dried in air at room temperature; the above synthesis yielded approximately 1 g of HAp. The samples were characterized by X-ray diffraction (XRD), transmission electron microscopy (TEM), and Fourier transform infrared (FTIR) spectroscopy. Surface area determination was performed by single point BET analysis (N_2 adsorption).

III-2-b-ii Precipitation of hydroxyapatite at room temperature:

In this synthesis procedure, 500 mg of HAp were dissolved in 100 ml of 0.1 N HCl at 20 °C. This solution was diluted to 1000 ml with deionized water, yielding a solution that contained 5 mM Ca^{2+} with pH approx. 2.8. The solution was stirred gently and 0.5 M potassium hydroxide solution was added in drops to the calcium solution. The pH was raised to 7.5 by KOH additions. When the pH exceeded 7 the solution became supersaturated and HAp particles began to precipitate. The solution is left stirring during 30 mn, then the pH is raised to 8 by addition of KOH and was stirred overnight.

The final step involved titration of the solution in order to precipitate all of the remaining calcium phosphate. The pH of the solution was maintained at 8 by regular addition of KOH. This stepwise reaction favors growth of larger HAp crystals. The precipitate was vacuum filtered, washed with deionized water, and dried in air at room

temperature; this synthesis yielded approximately 450 mg of HAp. The samples were characterized by XRD, TEM, FTIR and BET.

III-2 Analyses:

III-2-a X-ray diffraction:

X-ray diffraction patterns were obtained using a Rigaku 250 mm diffractometer RU300 (18 kW) with a copper source. Spectra were obtained from the diffraction of Cu K α radiation at wavelength $\lambda=1.540598 \text{ \AA}$. The spectra were collected between 20° and 55° (degrees 2θ) in step scan mode with a step size of 0.004° and a count time of 0.5 s.

Each sample from the hydrothermal synthesis was shown to be well-crystalline hydroxyapatite, although the degree of crystallinity varied according to preparation conditions; in general, samples prepared at higher temperature had higher degree of crystallinity. The values of d were consistent with the hexagonal space group P6₃/m with a=0.9418 nm and c=0.6884 nm (Table III-2).

	a (nm)	c (nm)
HAp 220 °C	0.9415	0.6874
HAp 170 °C	0.9424	0.68842
HAp 130 °C	0.9431	0.6887

Table III-2: Crystallographic parameters for hydroxyapatite.

Figure III-1 shows the diffraction patterns obtained for the precipitates prepared at 130 °C, 170 °C and 220 °C. For the sample at 220°C, the sharp, well-resolved peaks indicate that the precipitates are pure, crystalline Hap, while at lower temperatures the (211) and (112) peaks are not well-resolved, and are hardly discernable in the sample prepared at 130°C.

The XRD of the precipitated HAp is consistent with that of hydrothermally-synthesized Hap, but this sample appears to be much less crystalline. The presence of some well-resolved high-angle diffraction (approx. 46.9 °, 49.8 °, and 53.5 °) peaks suggests that the material is crystalline but the broadness of the peaks suggests that this sample is probably poorly crystallized.

A small amount of a second calcium phosphate phase is also present in several spectra (HAp 130 °C and HAp 220 °C). The peaks at 31 ° and 34.4 ° do not belong to the hydroxyapatite spectrum, and they are identified as the highest intensity peaks from whitlockite, or tricalcium phosphate (TCP). The composition of TCP is $\text{Ca}_3(\text{PO}_4)_3$, so that Ca/P ratio is 1.5, close to the 1.67 stoichiometric ratio of hydroxyapatite. Tricalcium phosphate has proposed to be a precursor in the synthesis of hydroxyapatite [14], which is the thermodynamically stable calcium phosphate under the reaction conditions. However, in the present mode, the synthesis of HAp does not appear to proceed via the TCP precursor phase as shown in Figure III-2. After one hour of reaction, the main phase present is already HAp and the only other phase present in a significant amount is monetite (M). The presence of TCP or M impurities is likely due to a non stoichiometry of the initial solution.

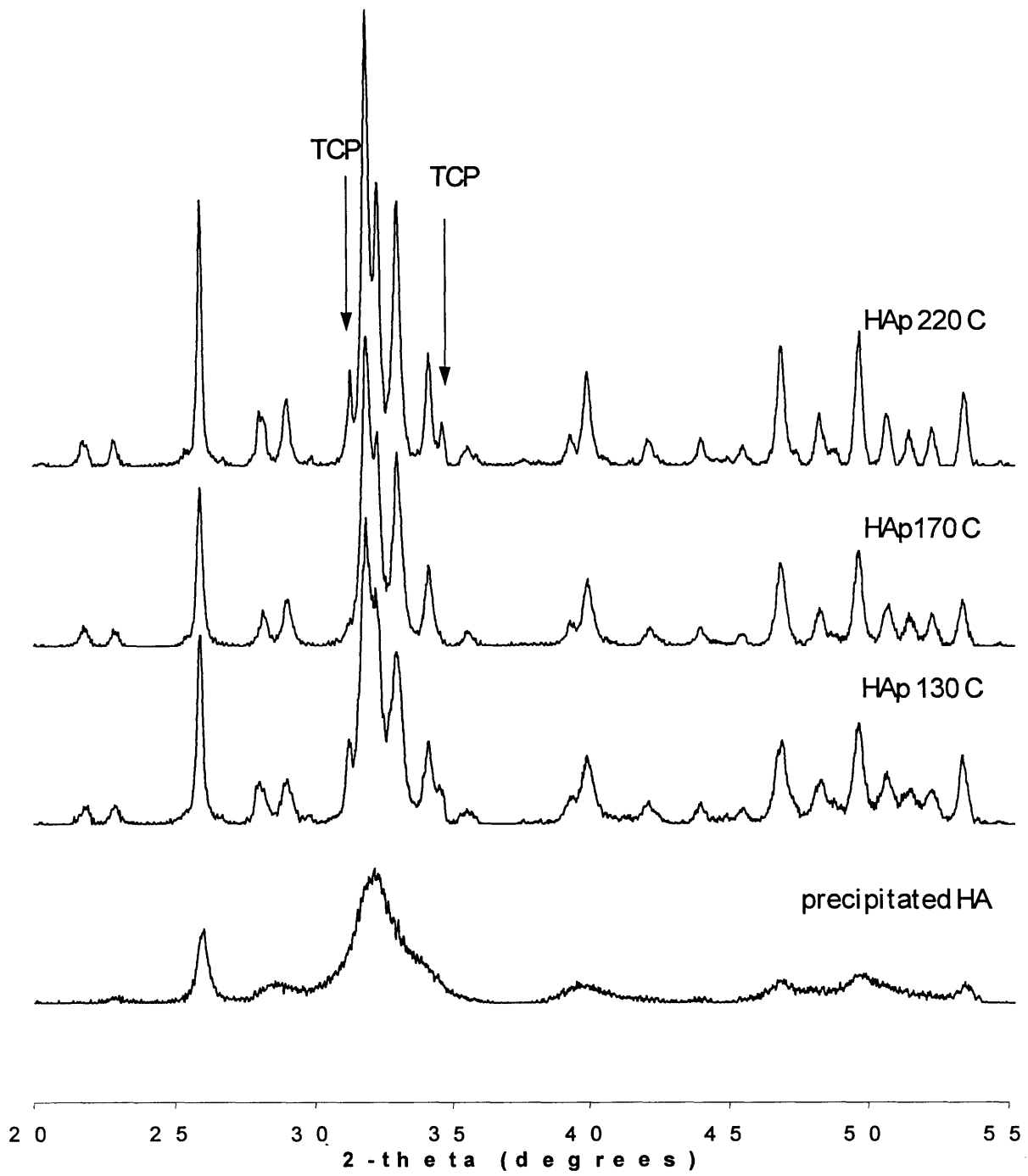


Figure III-1: XRD spectra for HAp 130, 170, 220 °C, and precipitated.

III-2-b Infrared spectrometry (FTIR):

Fourier transform infrared spectra were obtained using a Nicolet Impact 410 spectrometer with Omnic software. Samples were prepared as KBr disks.

The FTIR spectra of the hydrothermally-synthesized HAp (figure III-3) are characteristic of hydroxyapatite, showing PO_4^{3-} vibrational modes at 1087 cm^{-1} , 1046 cm^{-1} , 962 cm^{-1} , 605 cm^{-1} , and 565 cm^{-1} ; a OH stretch at 3570 cm^{-1} ; and a weak OH librational mode at 630 cm^{-1} . Broad peaks at $1370\text{-}1660\text{ cm}^{-1}$ and bands at 880 cm^{-1} were indicative of the carbonate (CO_3^{2-}) substitution for phosphates and hydroxyl groups which arises due to exposure to atmospheric CO_2 during the synthesis. The FTIR spectra illustrate the influence of the reaction temperature on HAp. Lower reaction temperatures lead to reduced intensities of the two characteristic OH bands (3570 cm^{-1} and 630 cm^{-1}) as well as an increase in the intensity of the carbonate peak ($1370\text{-}1660\text{ cm}^{-1}$). In addition, the samples prepared at lower reaction temperatures contain a poorly resolved phosphate peak at 1090 cm^{-1} . For the precipitated Hap, the vibrational OH mode at 630 cm^{-1} is not resolved and the 3570 cm^{-1} peak is very weak. The peaks in the carbonate region ($1370\text{ cm}^{-1}\text{-}1600\text{ cm}^{-1}$) are broadened and a new peak (1500 cm^{-1}) characteristic of carbonate substitution has appeared. The intensity of the carbonate peak at 880 cm^{-1} and the poor resolution of some of the phosphate peaks ($1040\text{ cm}^{-1}\text{-}1090\text{ cm}^{-1}$) also confirms the increased carbonate content of this sample.

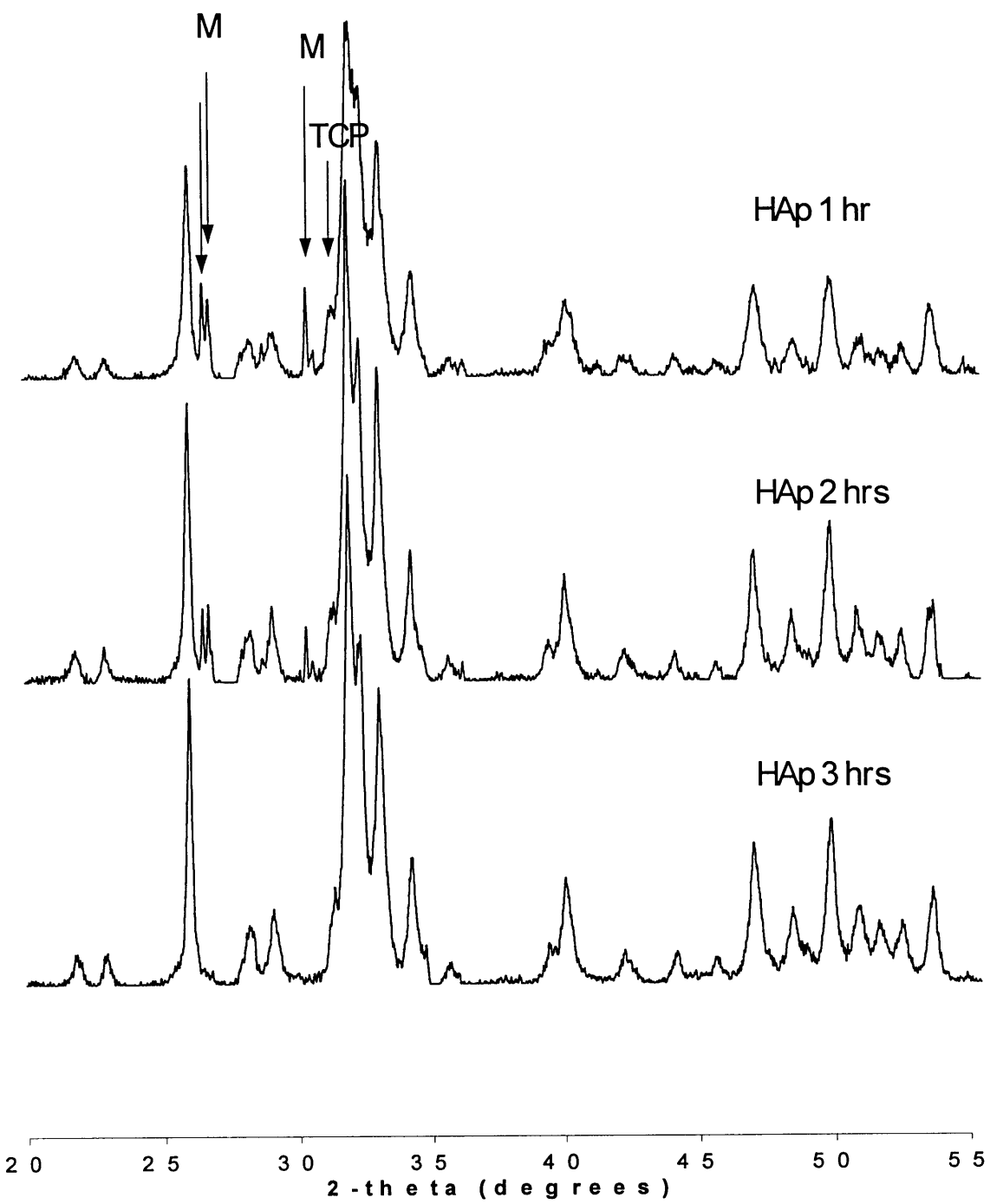


Figure III-2: Time dependence of the hydrothermal synthesis at 170 °C.

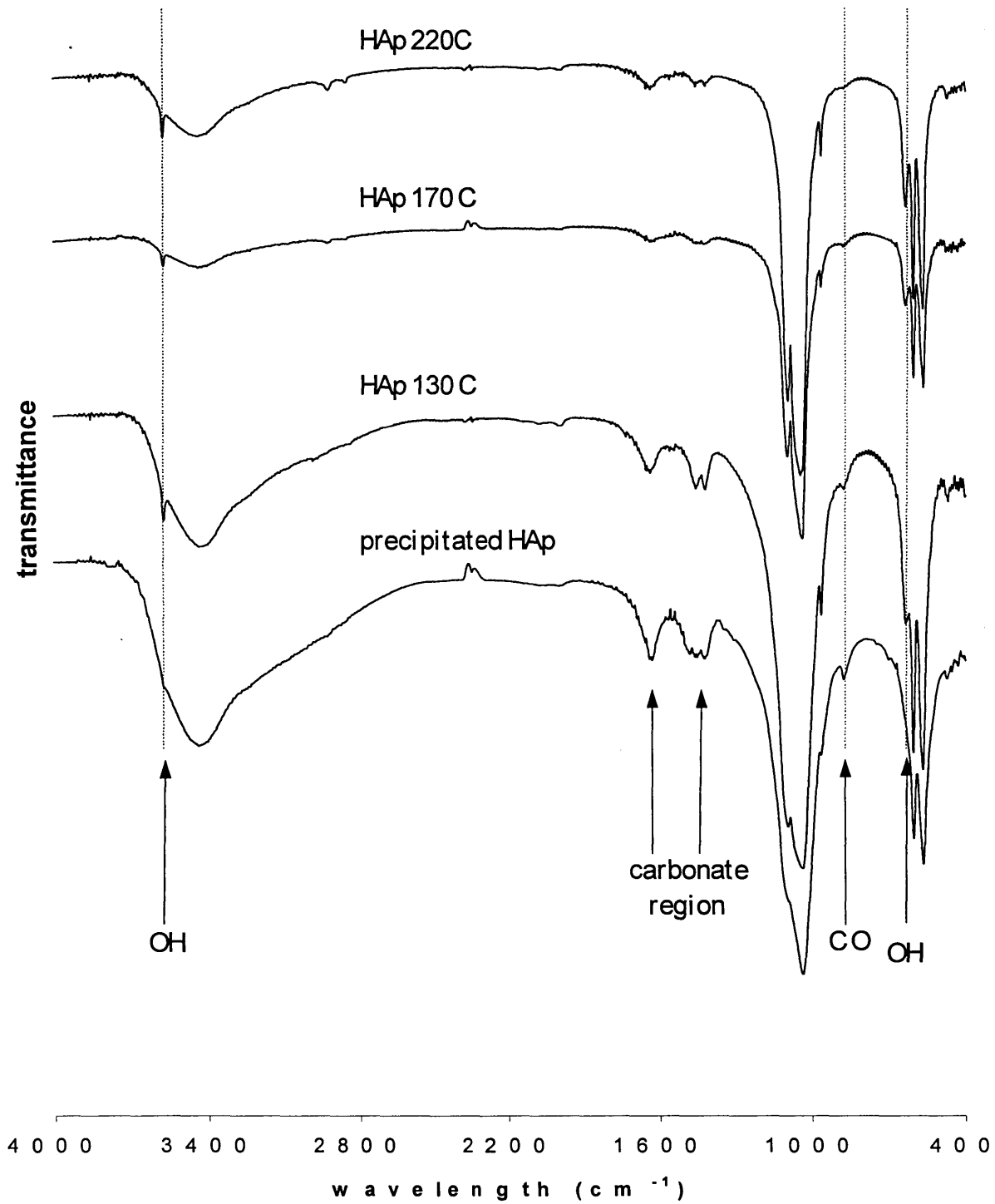


Figure III-3: FTIR spectra of HAp 130 °C, 170 °C, 220 °C and precipitated.

III-2-c TEM micrography:

TEM was performed using a JEOL 2000 FX at an operating voltage of 200 kV. Sample preparation involved dispersing the powder in isopropanol by ultrasonication and evaporation of the suspension on 3 mm carbon-coated copper grids.

Electron micrographs of HAp (Figure III-4 to III-7) showed that the samples synthesized at high temperatures consisted primarily of columnar particles (10-30 nm width and 40-200 nm length) with a few needle-like crystals. The higher the temperature, the more needle-like were the crystals. In the case of HAp precipitated, the structure was much less regular. The sample presents some elongated shapes but no apparent order or uniformity between the particles.

III-2-d Determination of surface area:

The surface area of the samples were determined by single point BET nitrogen adsorption method (30/70, N₂/He Quantasorb, Quantachrome). Samples synthesized at higher temperatures had lower surface areas, which suggests that larger particles were formed at higher temperatures.

Reaction temperature (°C)	Surface area (m ² /g)
130	45
160	37
190	33
220	25

Table III-2: Influence of the synthesis temperature on sample surface area.



Figure III-4: HAp 130 °C

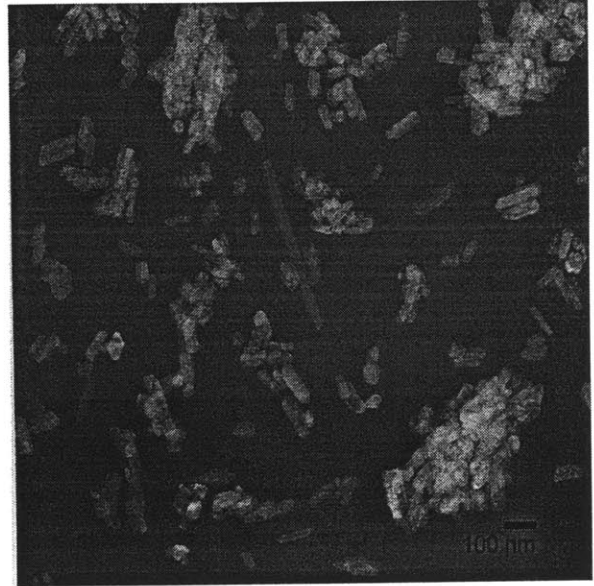


Figure III-5: HAp 170 °C

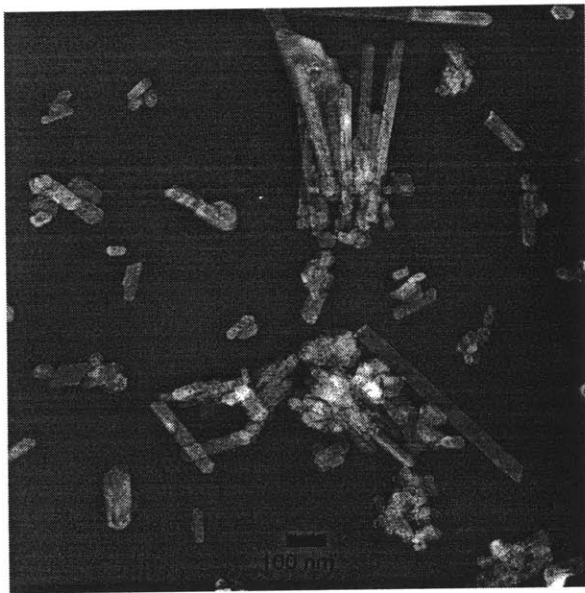


Figure III-6: HAp 220 °C

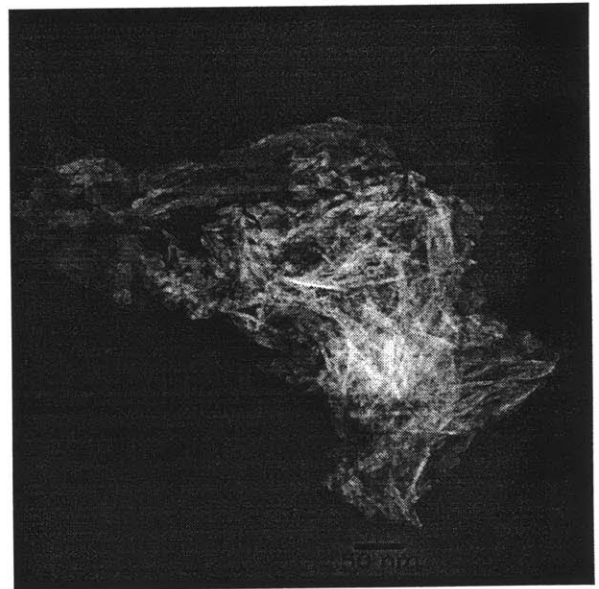


Figure III-7: HAp precipitated

III-3 Discussion:

The synthesis temperature appears to have a strong influence on the crystallinity of the hydroxyapatite sample. At lower temperatures, X-ray powder diffraction shows a decrease in intensity and an increase in width of the diffraction peaks due to a lower crystallinity of the samples. BET results are consistent with this observation that a decrease in crystallinity at lower synthesis temperature is correlated to a smaller particle size.

Moreover, the FTIR spectra suggest that hydroxyapatite precipitated at lower temperatures has a greater extent of carbonate substitution. There are two types of substitution for hydroxyapatite (paragraph III-1): type A substitutions (CO_3^{2-} for OH^-) and type B substitutions (CO_3^{2-} for PO_4^{3-}).

In our samples, the decrease in the intensity of the OH vibrational modes (3570 cm^{-1} and 630 cm^{-1}) and of the phosphate peaks (1087 cm^{-1}), in conjunction with increased intensities of the carbonate peaks (1370 cm^{-1} - 1600 cm^{-1} , and 880 cm^{-1}) indicate that low-temperature syntheses yield carbonate-substituted apatites. HAp synthesized by the precipitation method exhibits this characteristic behavior. Moreover, these observations are consistent with the observation that carbonate substitution in apatites reduces the crystal size and changes the morphology from needles to platelets [14].

IV- Incorporation of amino-acids:

Inspired by the observation that intracrystalline proteins are present in biogenic minerals such as nacreous aragonite (CaCO_3) in mollusk shells, the goal of this work was to prepare HAp samples that contain intracrystalline organic inclusions. The first step was to use amino acids, which are the basic building blocks of proteins, and to study the effects of charge and side chain functionality (R) on crystallization of HAp. Samples were characterized using XRD, FTIR and TEM.

IV-1 Materials and methods:

Amino acids were used as received from Aldrich (USA).

The synthesis of HAp at 170 °C was performed as described in section II-2-b, with 0.01 mole of the organic species added to the phosphoric acid solution prior to addition of calcium hydroxide.

Experiments inducing adsorption under the conditions of synthesis of HAp were conducted to differentiate surface adsorbed amino acids from the entrapped, intracrystalline ones. During these experiments, 0.01 mole of the organic species was added to the phosphoric acid solution. Then, the pH was raised to 12 and 1 g of HAp previously synthesized at 170 °C was added to the solution in a 23 ml Teflon™ cup. The Teflon™ cup was sealed in a digestion bomb and placed in the oven at 170 °C for 24 hours.

Amino acids can be categorized into five main categories according to R group: nonpolar, aliphatic R groups; aromatic R groups; positively-charged R groups; negatively-charged R groups; polar, uncharged R groups. One amino acid was chosen

from each group (Figure IV-1). The amino acids are depicted in the protonation state that is expected to be present under the pH conditions of the synthesis (pH 12).

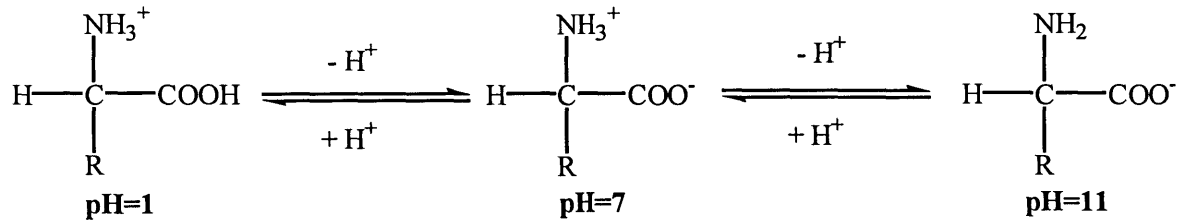


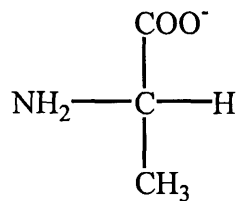
Figure IV-1: pH-dependant ionization states of amino acids.

IV-2 Results:

IV-2-a Alanine:

- Nonpolar aliphatic R groups:

Hydrocarbon side chains are nonpolar and hydrophobic. **Alanine** (R=CH₃) (1), valine (R=CH₂CH₂CH₃), leucine (R=CH₂CH₂CH₂CH₃), isoleucine (R=CH₂CH(CH₃)CH₃), glycine (R=H) and proline (R=C₃H₆ ring conformation) are commonly located in the hydrophobic region of a globular protein structure.



(1)

- Results:

The XRD and FTIR spectra of hydroxyapatite synthesized in the presence of alanine do not differ from that of pure HAp synthesized under the same conditions (Figure IV-2 and Figure IV-3). The XRD spectrum is characteristic of pure hydroxyapatite with a small amount content of tricalcium phosphate $\text{Ca}_3(\text{PO}_4)_2$ (TCP) as it is shown Figure IV-3. As FITR can detect materials at levels below 0.1 wt% to 1 wt% [15] if a significant quantity of alanine were adsorbed or entrapped, characteristic peaks from the amino acid functionalities or the R group would be expected. However, IR bands corresponding to alanine do not appear to be present. Therefore the amount of alanine which interacts with the inorganic matrix is small and not discernable. TEM images of the crystals also suggest that alanine does not significantly affect the synthesis, since the crystals synthesized in the presence of alanine are similar in shape (needle-like) to pure HAp (Figure IV-4 and Figure IV-5).

IV-2-b Phenylalanine:

- Aromatic R groups:

Phenylalanine ($\text{R}=\text{C}_6\text{H}_5$), tyrosine ($\text{R}=\text{CH}_2\text{C}_6\text{H}_4\text{OH}$) and tryptophan ($\text{R}=\text{CH}_2\text{C}_2\text{NH}_2\text{C}_6\text{H}_5$) are relatively nonpolar (hydrophobic) due to the aromatic side chains, although tyrosine is somewhat polar because of the hydroxyl group.

The aromatic side groups are responsible for the characteristic strong absorbance of light ($\lambda=280\text{ nm}$) by proteins.

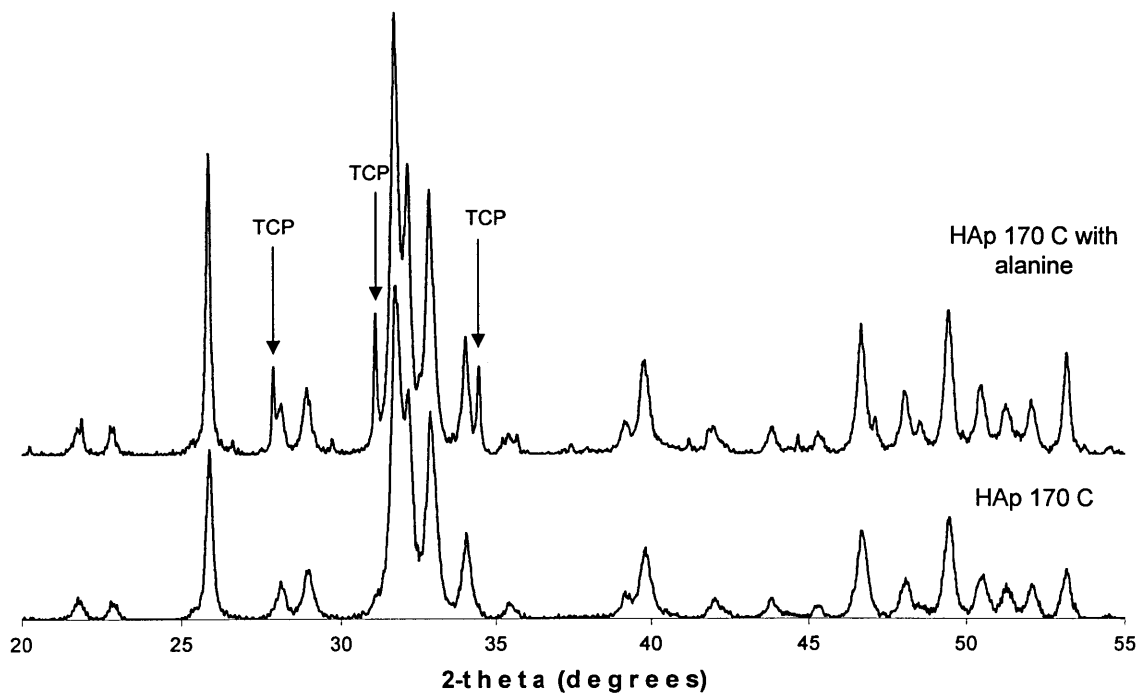


Figure IV-2: Influence of alanine on the XRD spectrum of HAp at 170 °C.

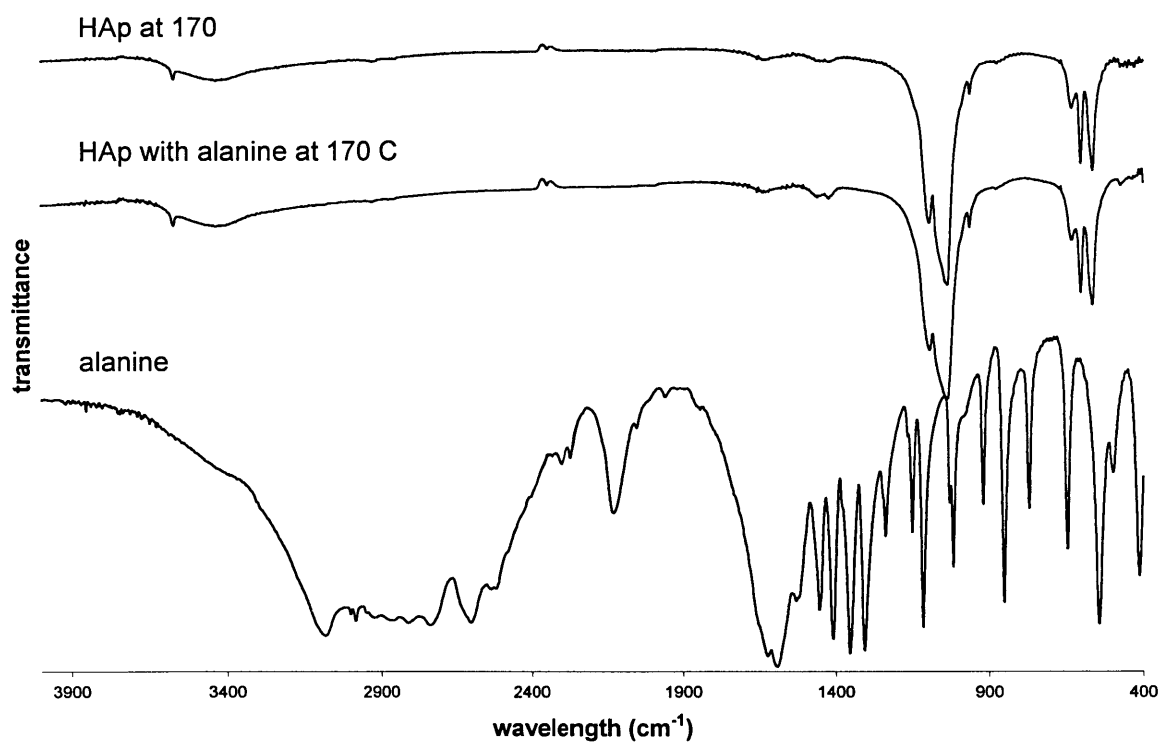


Figure IV-3: Influence of alanine on the FTIR spectrum of HAp at 170 °C.

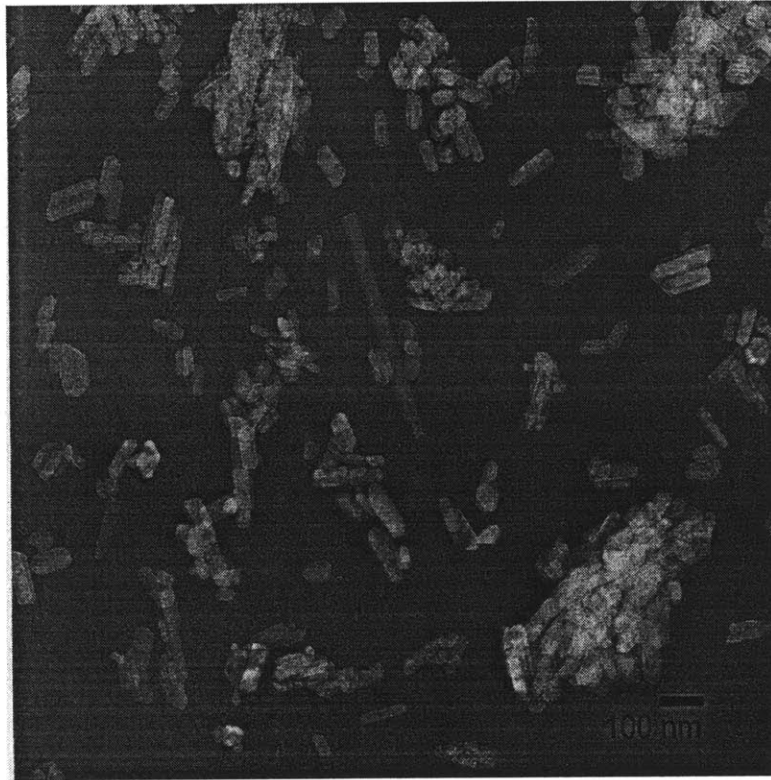


Figure IV-4: HAp 170 °C.

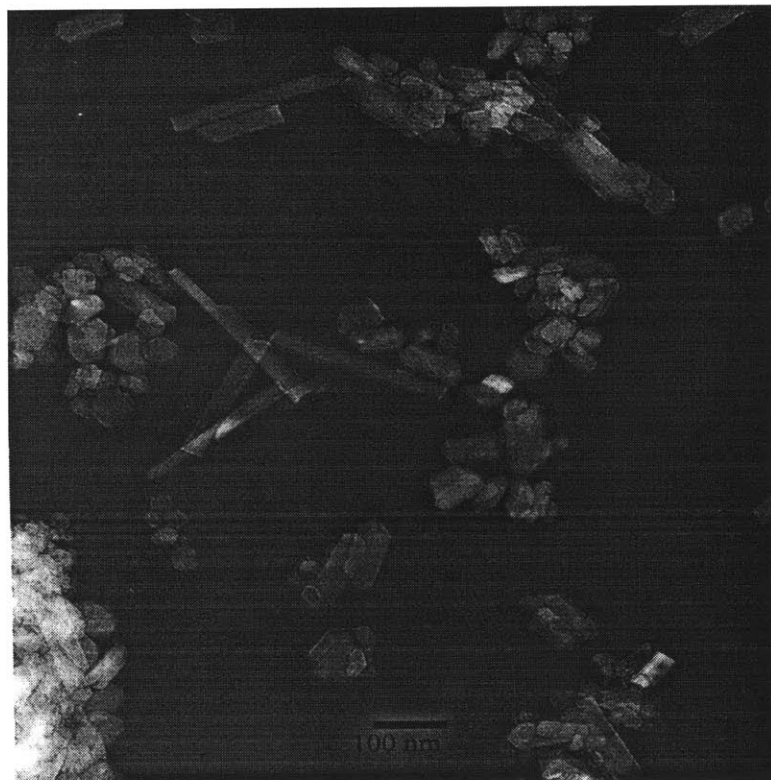
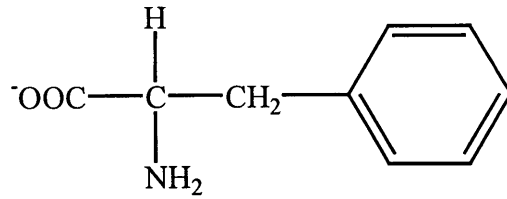


Figure IV-5: HAp 170 °C with alanine.



(2)

- Results:

The XRD spectrum of HAp synthesized in the presence of phenylalanine (Figure IV-6) indicates that HAp and additional calcium phosphate phases (monetite (M) CaPO₃(OH) and tricalcium phosphate (TCP) Ca₃(PO₄)₂) are present in the sample. Both of the new mineral phases account for smaller stoichiometric Ca/P ratio: 1 for monetite and 1.5 for tricalcium phosphate. The addition of phenylalanine also seems to affect the crystallinity of the HAp, since the peaks in the XRD spectrum of the sample synthesized with phenylalanine are not well-resolved.

The FTIR spectrum indicates that the amino acid is present either on the surface of the product or entrapped in the matrix (Figure IV-7). Resonances at 1580 cm⁻¹-1610 cm⁻¹ and 1400 cm⁻¹-1510 cm⁻¹ are indicative of the NH₂ group and the COO⁻ antisymmetric stretches and match the highest intensity peaks in the spectrum of phenylalanine. To test whether phenylalanine can adsorb in significant quantities on HAp, the reaction conditions under which HAp with phenylalanine was synthesized were reproduced using HAp and pure adsorbate. The FTIR spectrum (Figure IV-8) of the

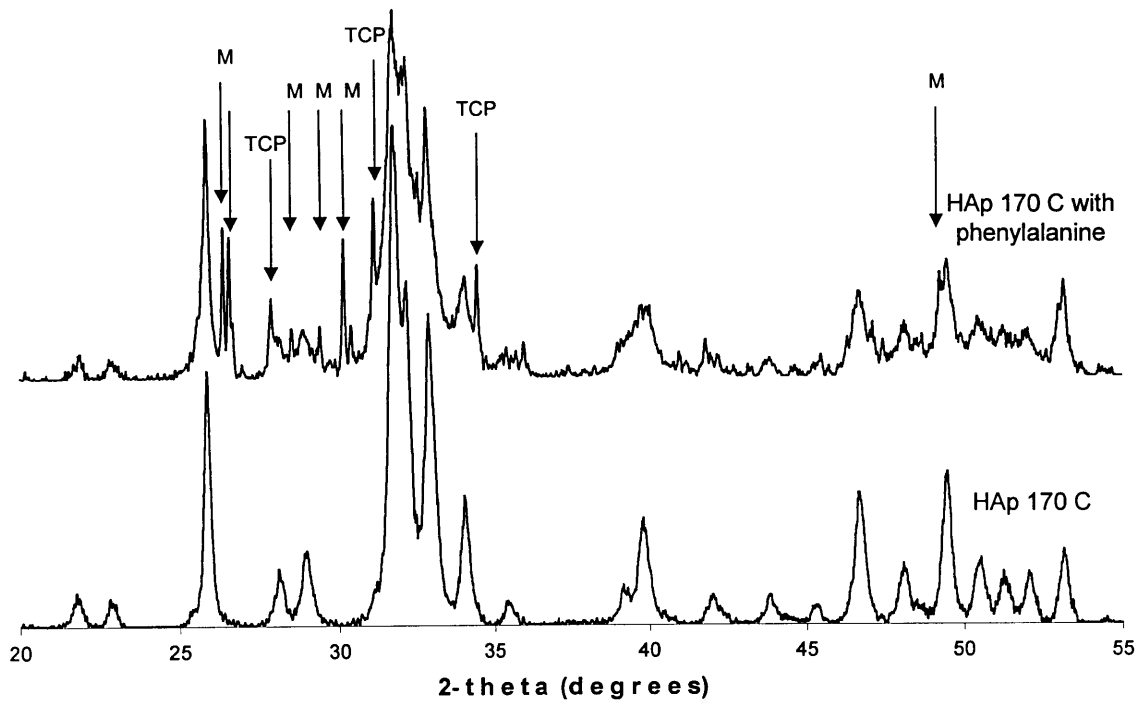


Figure IV-6: Influence of phenylalanine on the XRD spectrum of HAp at 170 °C.

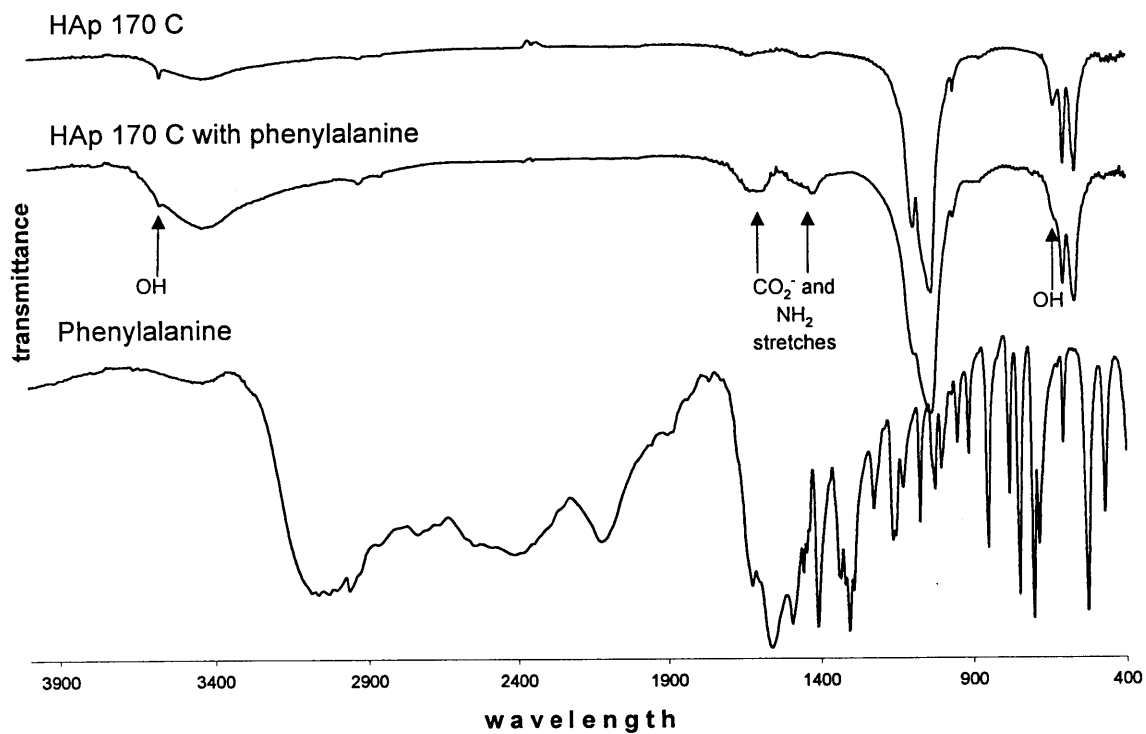


Figure IV-7: Influence of phenylalanine on the FTIR spectrum of HAp at 170 °C.

product of the adsorption experiment does not indicate a significant organic content, which suggests that most of the phenylalanine that is present in the original sample is entrapped in the organic matrix.

However, the decrease in the intensity of the OH peaks in FTIR spectrum and the presence of additional phases in the XRD spectrum indicate that other calcium phosphate phases have been synthesized. These new phases are monetite and tricalcium phosphate. Both of the new minerals account for smaller stoichiometric Ca/P ratio, 1 for monetite and 1.5 for whitlockite.

TEM micrographs (Figure IV-9 and Figure IV-10) reveal irregular and non-uniform crystal habits rather than uniform columnar and needle-like particles of pure HAp.

IV-2-c Threonine:

- Polar uncharged R groups:

The R groups of these amino acids Serine (CH_2OH), **threonine** ($\text{CH}(\text{CH}_3)(\text{OH})$) (3), cysteine (CH_2SH), methionine ($\text{CH}_2\text{CH}_2\text{SHCH}_3$), asparagine ($\text{CH}_2\text{CO}(\text{NH}_2)$) and glutamine ($\text{CH}_2\text{CH}_2\text{CO}(\text{NH}_2)$) are more hydrophilic due to their polar hydrogen-bonding functional groups. For example, serine and **threonine** contain a hydroxyl group, cysteine and methionine contain a sulfur atom, and asparagine and glutamine contain an amide group.

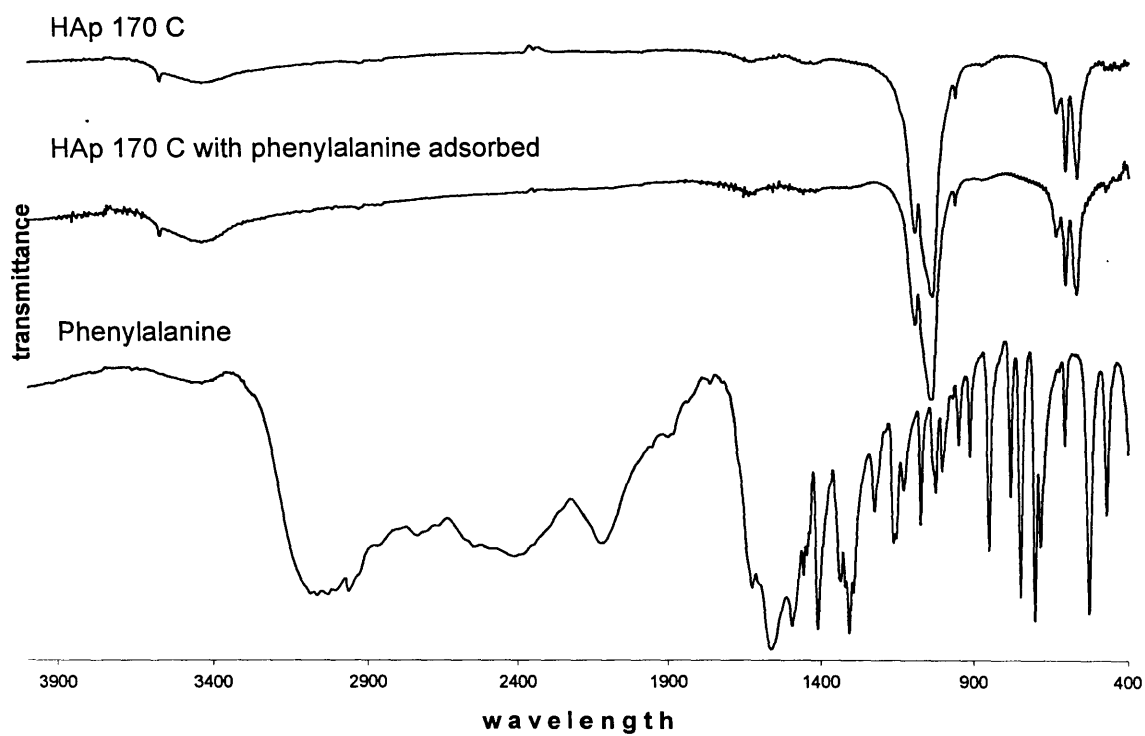


Figure IV-8: Influence of the adsorption of phenylalanine on the FTIR spectrum of HAp at 170 °C.

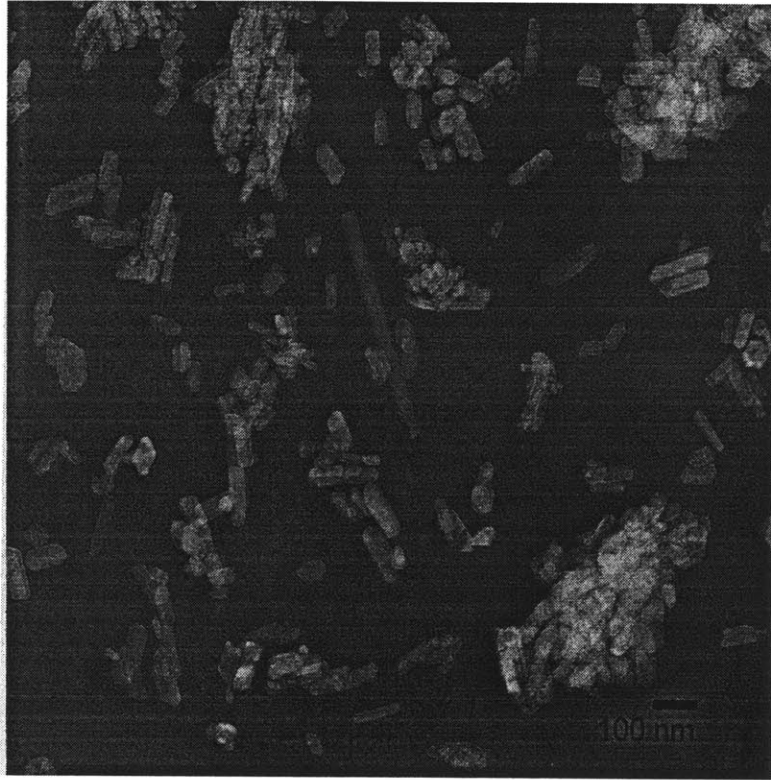


Figure IV-9: HAp 170 °C.

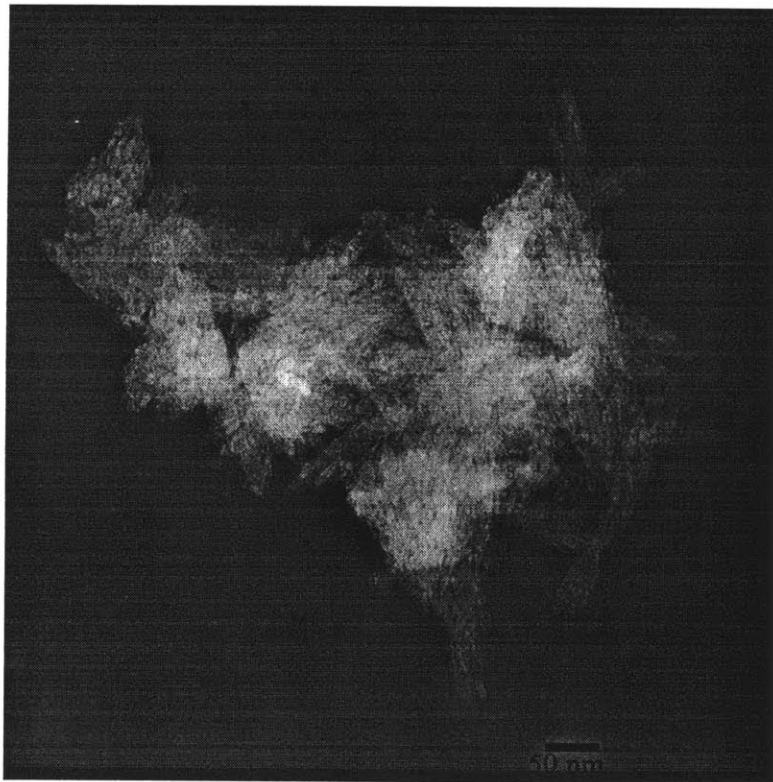
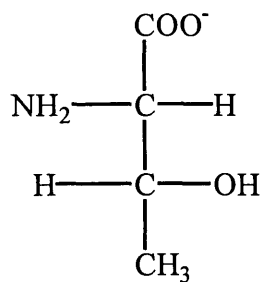


Figure IV-10: HAp 170 °C with phenylalanine.



(3)

- Results:

The XRD spectrum of HAp synthesized in the presence of threonine (Figure IV-10) indicates that, in addition to HAp, other calcium phosphate phases, monetite and tricalcium phosphate are formed. In fact, in this case, monetite is almost exclusively formed. Both of the new mineral phases account for smaller stoichiometric Ca/P ratio. The addition of threonine also seems to affect the crystallinity of the HAp, since the peaks are less-resolved and have a lower their intensity.

As in the case of phenylalanine, the FTIR and XRD spectra suggest that there is a strong interactions between the amino acid and the inorganic components during the synthesis. The FTIR spectrum (Figure IV-11) shows a decrease or disappearance in the intensity of the OH bands, which the presence of other calcium phosphate phases (TCP and monetite) or a highly substituted carbonate apatite. The observation of Figure IV-11 shows the apparition of several strong peaks at 1640 cm^{-1} and 1430 cm^{-1} . Since at $170 \text{ }^\circ\text{C}$ the carbonate content of hydroxyapatite should be low, the peaks in the carbonate region of the sample synthesized with threonine are likely due to the presence of threonine that

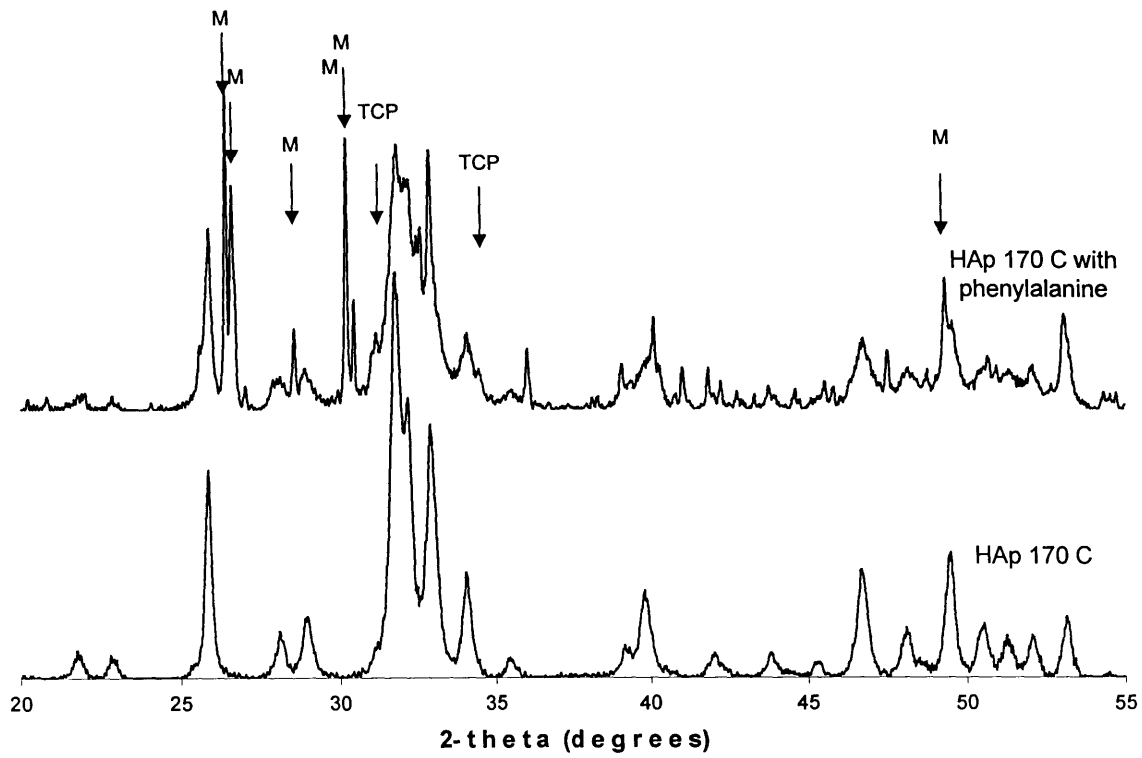


Figure IV-10: Influence of threonine on the XRD spectrum of HAp at 170 °C.

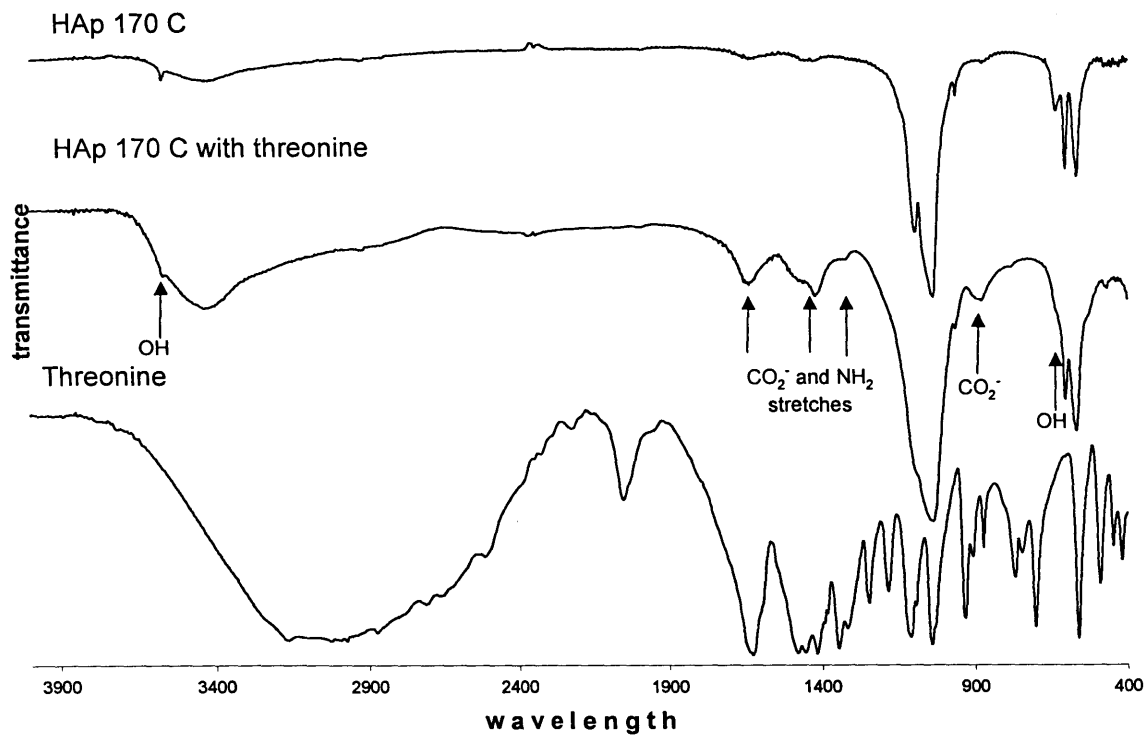


Figure IV-11: Influence of threonine on the FTIR spectrum of HAp at 170 °C.

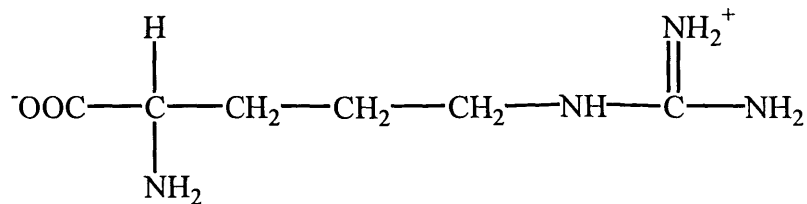
has been entrapped or adsorbed on the surface. The FTIR spectrum (Figure IV-12) of the product of the adsorption experiment of threonine on HAp does not contain strong evidence of amino acid peaks suggesting that most of the threonine that is present in the sample is entrapped in the organic matrix.

TEM micrographs (Figure IV-13 and Figure IV-14) also correlate the hypothesis that amino acid molecules interact with the inorganic components during crystallization since the crystals are highly irregular.

IV-2-d Arginine:

-Positively charged (basic) R groups:

Lysine ($\text{CH}_2\text{CH}_2\text{CH}_2\text{CH}_2\text{NH}_3^+$), **arginine** ($\text{CH}_2\text{CH}_2\text{CH}_2\text{NHC}(\text{NH}_2)(\text{NH}_2^+)$) (4), and histidine ($\text{CH}_2\text{C}_3\text{N}_2\text{H}_3$) have a net positive charge at pH=7 and are very hydrophilic due to their charged ionic side groups.



(4)

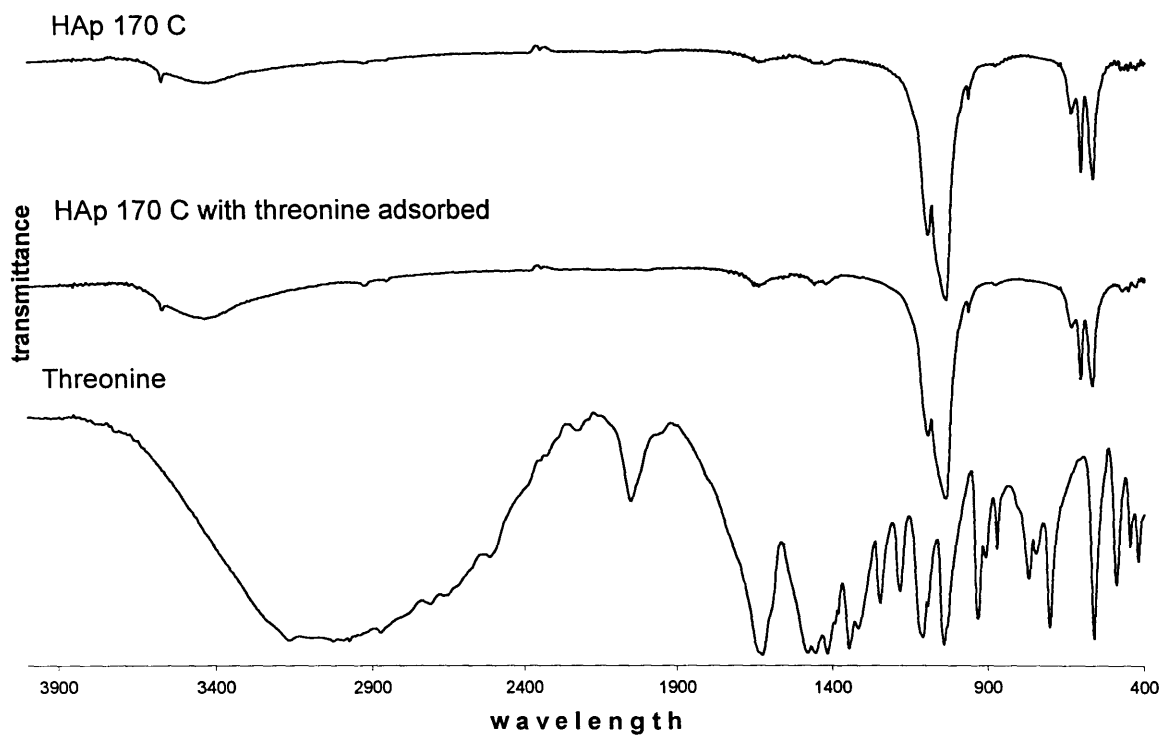


Figure IV-12: Influence of the adsorption of threonine on the FTIR spectrum of HAp at 170 °C.

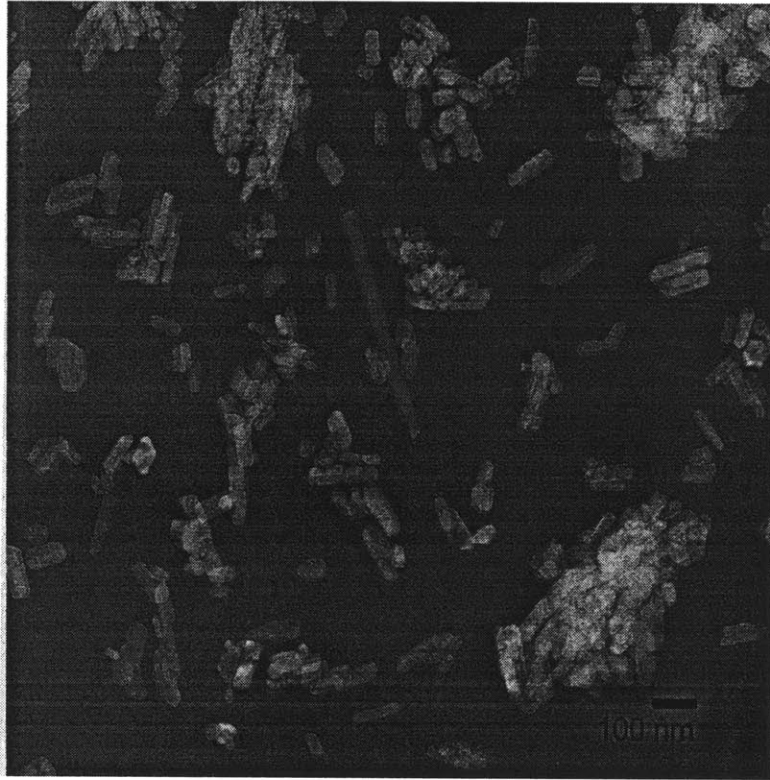


Figure IV-13: HAp 170 °C.

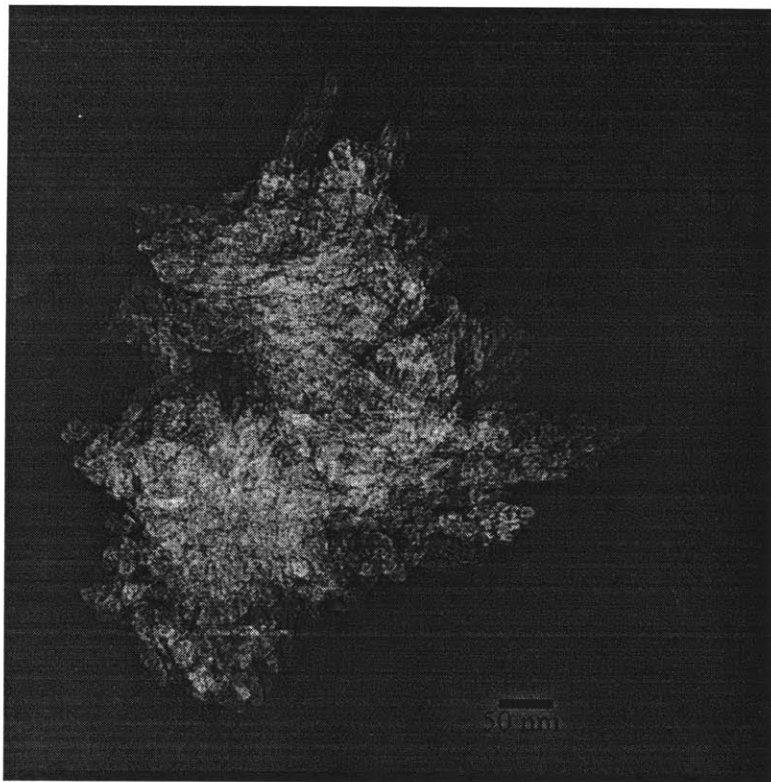


Figure IV-14: HAp 170 °C with threonine.

- Results:

The XRD and FTIR spectra of hydroxyapatite synthesized in the presence of arginine do not differ significantly from that of pure HAp synthesized under the same (see Figure IV-15 and Figure IV-16). The XRD pattern shows all the characteristics of pure hydroxyapatite. As FTIR can detect elements at levels below 0.1 wt% to 1 wt% if a significant quantity of arginine were adsorbed or entrapped, some of the characteristic peaks from the amino acid functional group or the R group would be expected. However, none of the characteristic vibrations of arginine are present in the FTIR spectrum. Therefore the amount of arginine which interacts with the inorganic matrix must be very small and not discernable. TEM micrographs also suggest that arginine does not significantly affect the synthesis since the particles have the same shape (columnar with some needles) as those pure HAp (Figure IV-15 and Figure IV-16).

IV-2-e Aspartic acid:

- Negatively charged (acidic) R groups:

The two amino acids that have R groups with a net negative charge at neutral or basic pH are **aspartic acid** (CH_2COOH) (5) and **glutamic acid** ($\text{CH}_2\text{CH}_2\text{COOH}$).

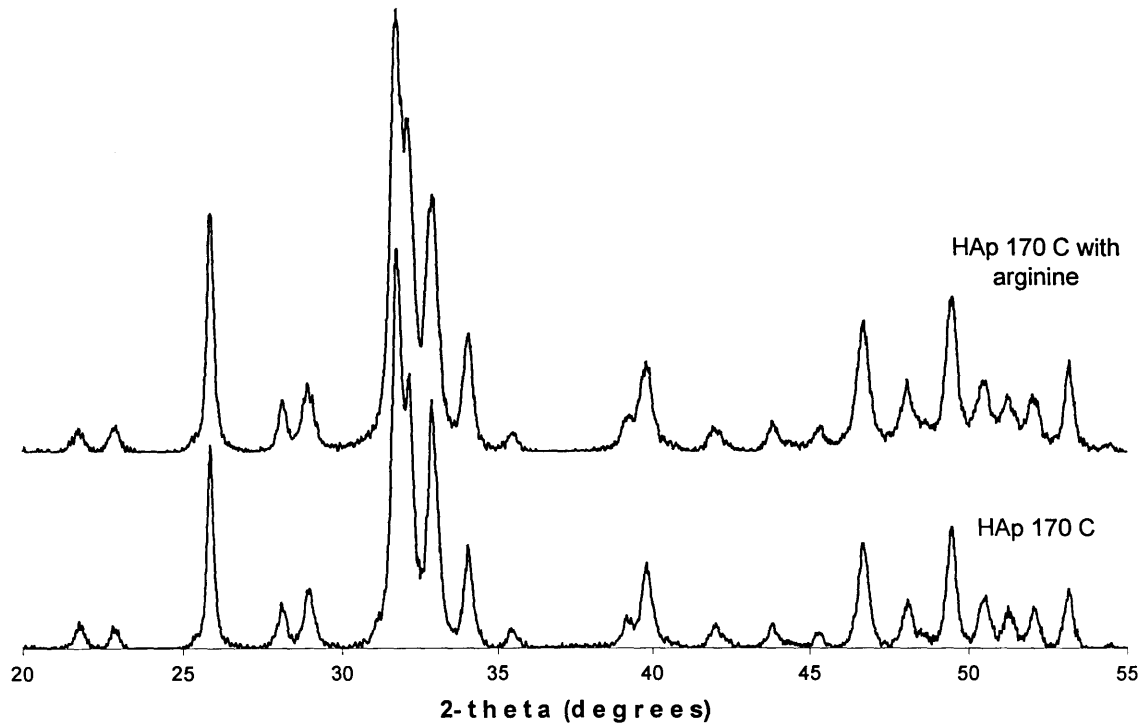


Figure II-14: Influence of arginine on the XRD spectrum of HAp at 170 °C.

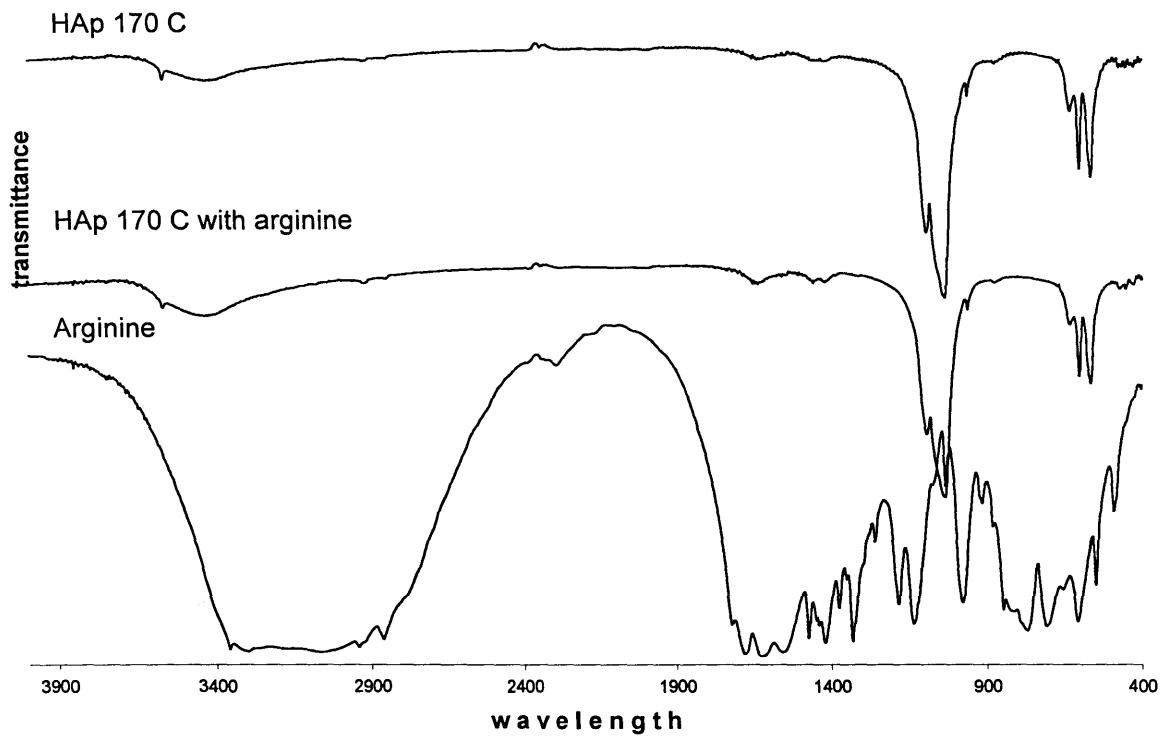


Figure II-15: Influence of arginine on the FTIR spectrum of HAp at 170 °C.

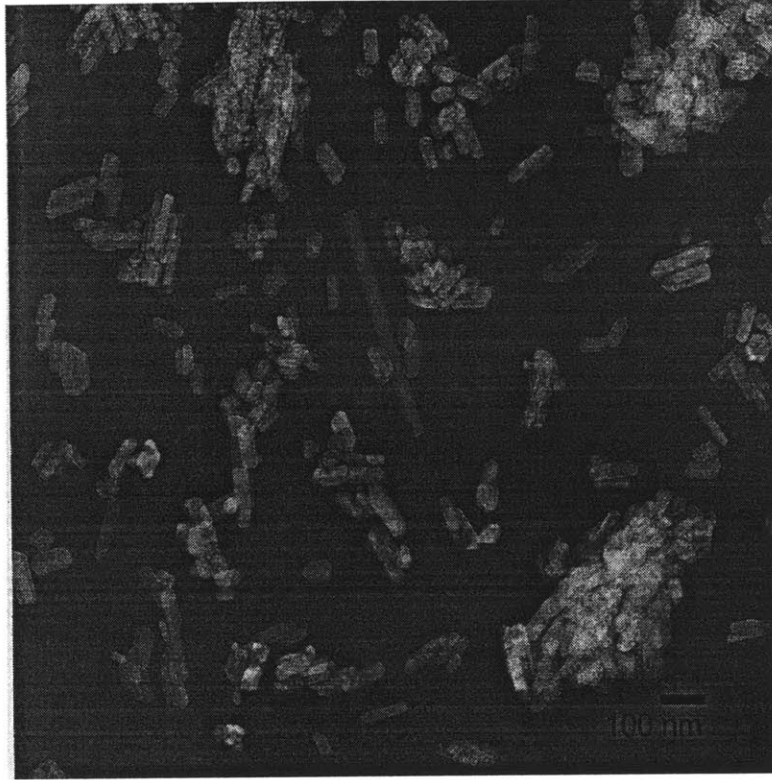


Figure IV-15: HAp 170 °C.

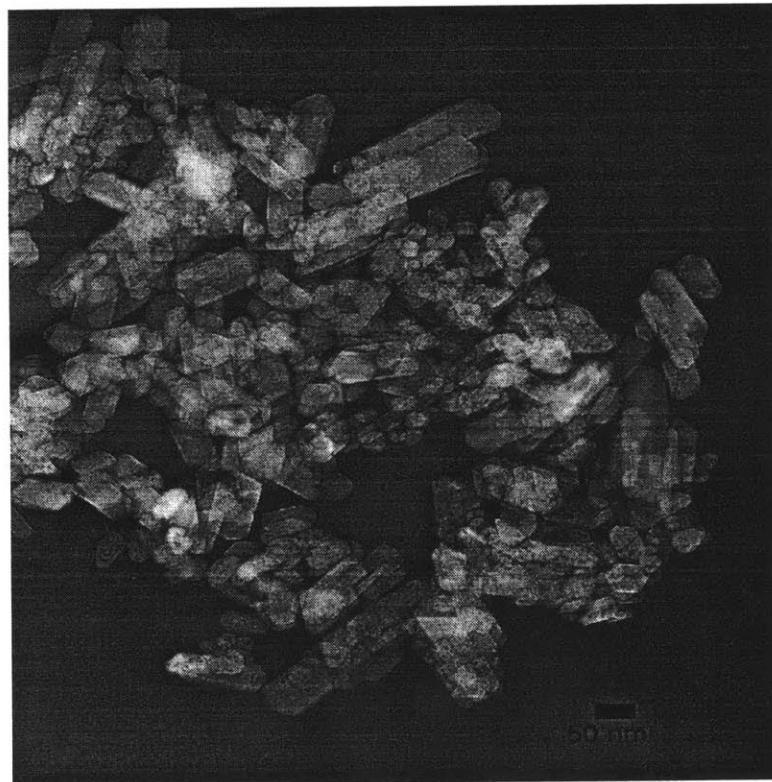
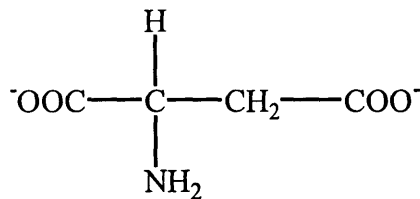


Figure IV-16: HAp 170 °C with arginine.



(5)

- Results:

The XRD spectrum of HAp synthesized in the presence of aspartic acid (Figure IV-17) indicates tricalcium phosphate is also present in the sample. This new mineral phases account for smaller stoichiometric Ca/P ratio: 1.5. The addition of aspartic acid also seems to affect the crystallinity of the HAp, since the peaks are not well-resolved.

As in the case of phenylalanine and threonine additives, there appears to be a strong interaction between the amino acid and the inorganic components during the synthesis. The FTIR spectrum (Figure IV-18) shows a decrease or disappearance in the intensity of the OH bands suggesting the presence of another other calcium phosphate phase (TCP) or a highly substituted carbonate apatite. Strong peaks are present in the carbonate region (1400 cm^{-1} - 1610 cm^{-1}). Since at $170 \text{ }^\circ\text{C}$ the carbonate content of hydroxyapatite should be low, the presence of these peaks is indicative of the NH_2 group and the COO^- antisymmetric stretches (1630 cm^{-1} and 1430 cm^{-1}) and suggests that a significant amount of aspartic acid has either been entrapped in the crystal or is adsorbed on the surface (1630 cm^{-1} and 1430 cm^{-1}). The FTIR spectrum (Figure II-19) of the product of the adsorption experiment does not contain organic peaks suggesting that most of the aspartic acid that is present in the original sample is entrapped in the organic

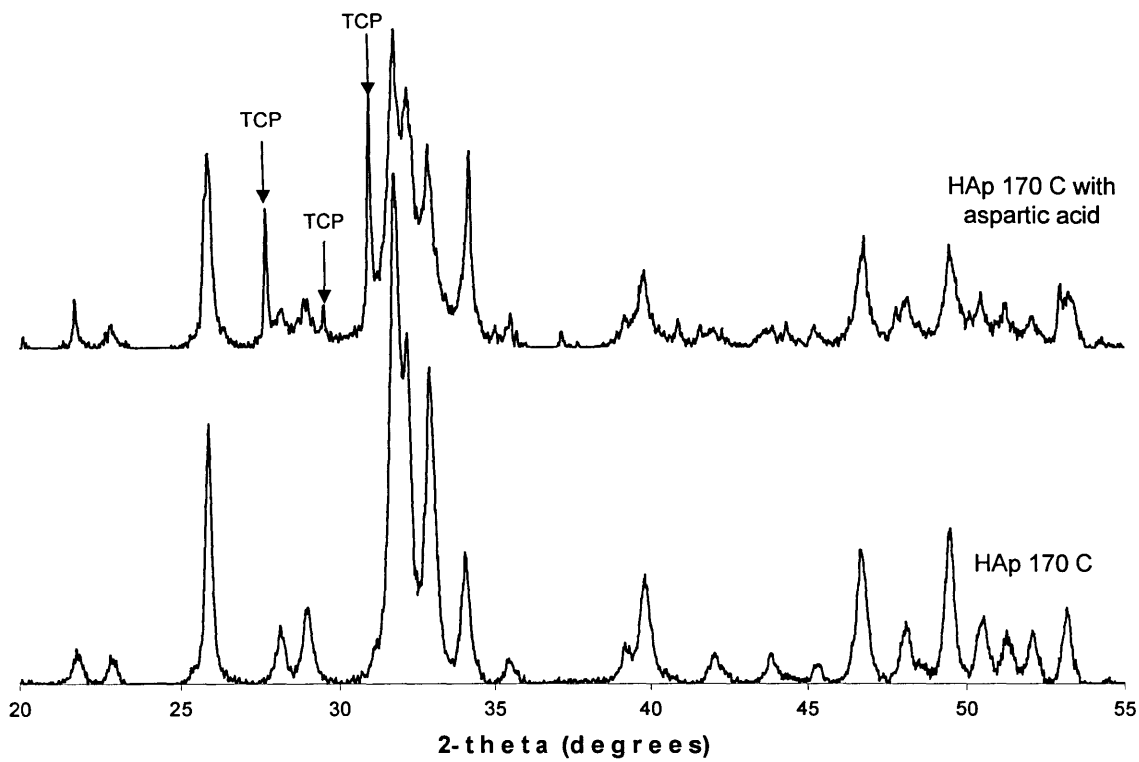


Figure IV-17: Influence of aspartic acid on the XRD spectrum of HAp at 170 °C.

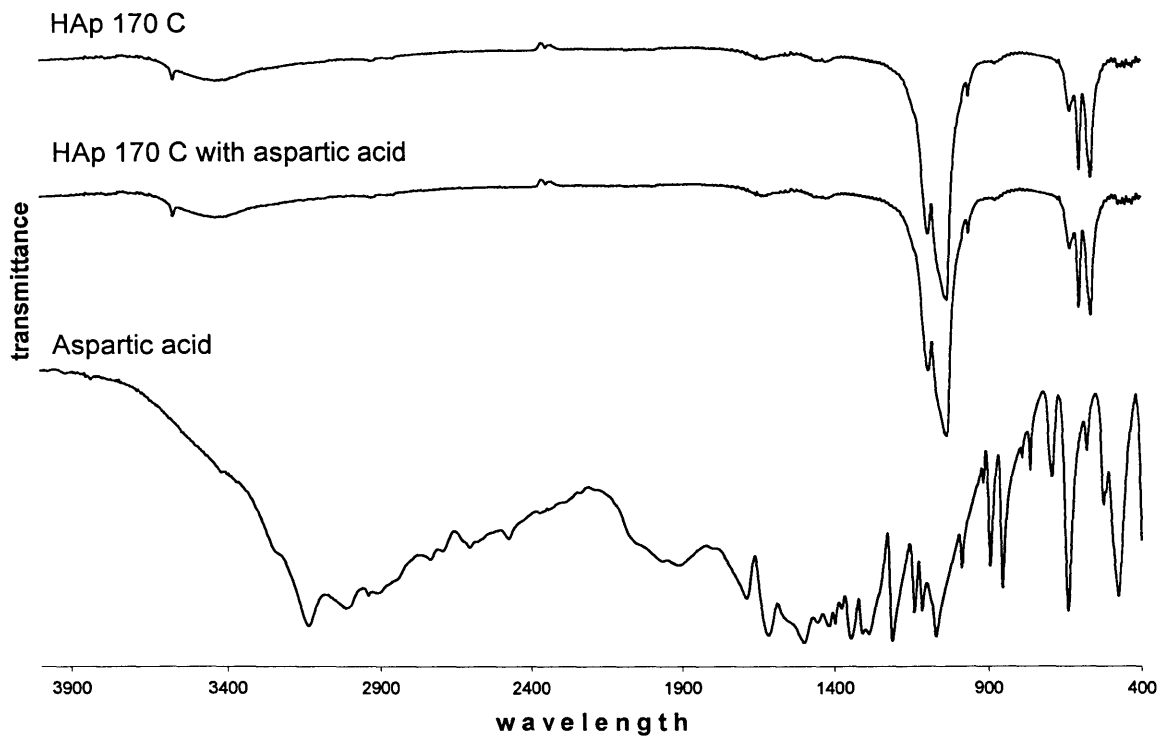


Figure IV-18: Influence of aspartic acid on the FTIR spectrum of HAp at 170 °C.

matrix (Figure IV-19).

TEM micrographs (Figure IV-19 and Figure IV-20) also correlate the hypothesis that amino acid molecules interact with the inorganic components during crystallization since the crystals are highly irregular.

IV-3 Discussion:

Three of the amino acids (phenylalanine, threonine, and aspartic acid) appear to have a significant influence on the synthesis of HAp. In these cases, the observation that a sufficient amount of amino acid to be detectable by FTIR cannot be adsorbed onto pre-formed HAp suggests that the amino acids present during the synthesis may be entrapped in the inorganic network. As all of the amino acids except for arginine are negatively-charged which is neutral, it was expected that there would be no adsorption on the HAp surface since the HAp surface is also negatively charged at pH 12. Electrostatic repulsions may prevent adsorption of the amino acids on the surface.

The presence of the amino acids also affects the synthesis in that they induce formation of new calcium phosphate phases, which have Ca/P ratios lower than that of HAp. This observation suggests that the amino acids may interact with the Ca^{2+} ions in the solution, which effectively lowers the ratio of free Ca^{2+} to PO_4^{3-} in the solution and leads to the formation of phases with lower Ca/P ratios such as TCP and monetite. Although phenylalanine sample contains both TCP and monetite impurities, the aspartic

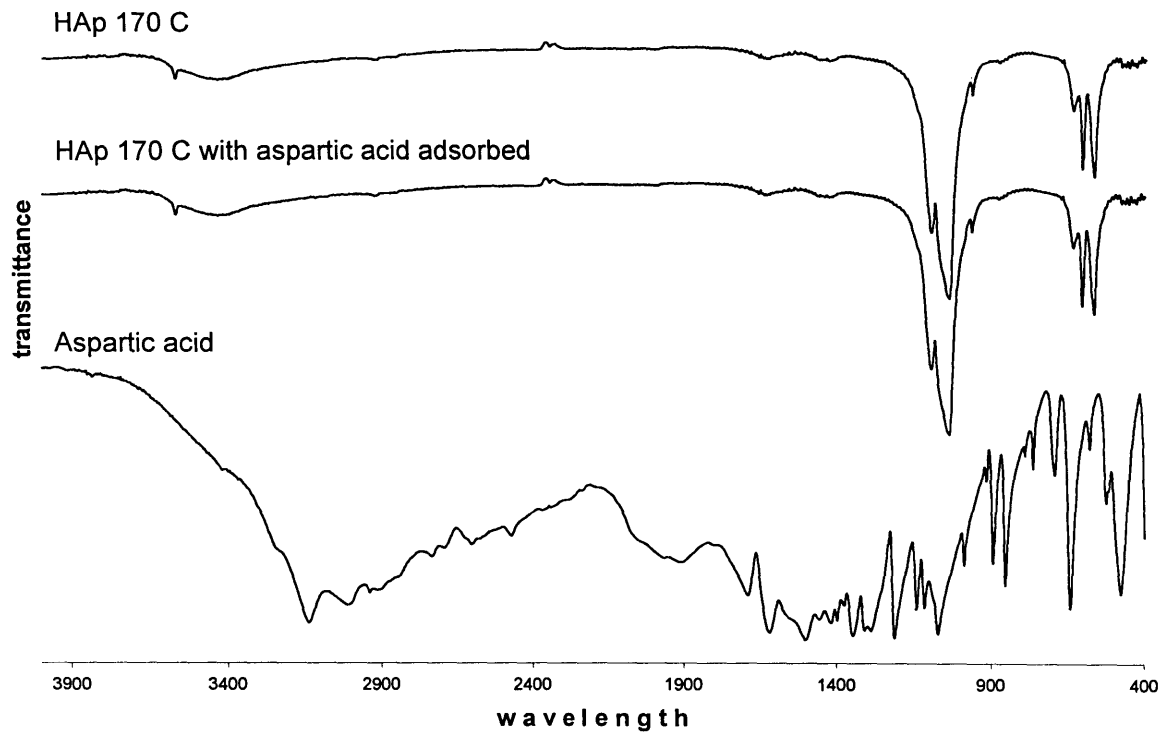


Figure IV-19: Influence of the adsorption of aspartic acid on the FTIR spectrum of HAp at 170 °C.

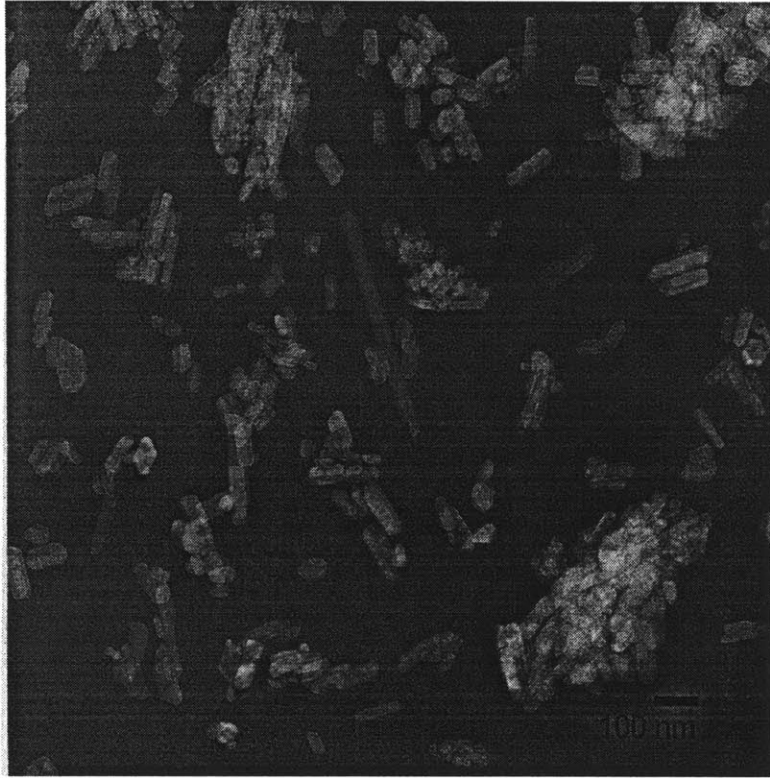


Figure IV-20: HAp 170 °C.



Figure IV-21: HAp 170 °C with aspartic acid.

acid sample contains TCP impurities and the threonine sample contains monetite impurities.

Among the other amino acids tested, alanine seems to interact weakly with the calcium ions which would justify the presence of TCP on the XRD impurities. However, the FTIR spectrum does not show any significant incorporation of the amino acid in the inorganic network. Arginine does not appear to have any significant effect on the synthesis of HAp.

One common characteristic is found among the four amino acids that affect the HAp reaction: the negative charge of the molecule. This correlates the hypothesis that the amino acid molecules interact specifically with the positively-charged calcium ions. The negatively-charged carboxyl groups are electrostatically attracted to the calcium ions in the solution, which inhibits the interaction of the Ca^{2+} ions with phosphate and hydroxyl groups to form HAp. Thus, the Ca/P ratio of the solution is effectively lowered, which leads to the formation of phases with lower calcium content. Although alanine is not entrapped within the Hap product and does not affect the crystal habits formed, the addition of alanine to the synthesis is characterized by an increase in TCP content of the product. Therefore the R chain of the amino acid probably plays a role in the entrapment process. Alanine has an aliphatic nonpolar side chain whereas aspartic acid and threonine have polar side chains due to a second carboxyl group for aspartate and a hydroxyl group for threonine. Both of these chains are likely to form ionic or hydrogen bonds. Aspartic acid can interact with one (chelate structure) or two calcium ions due to the presence of two carboxyl chains. Threonine may form some hydrogen bonds with some of the hydroxyl groups incorporating the inorganic network. This could explain why threonine

favors the formation of monetite which has a much higher OH/Ca ratio than HAp (1 versus 0.2). However, phenylalanine does significantly influence the synthesis of HAp although it has a nonpolar, aromatic side chain. By analogy to the structure of proteins which tends to minimize the surface area between nonpolar groups and the aqueous solution by excluding them from the surface, one hypothesis would be that under the reaction conditions the phenylalanine molecules would form some sort of micelles, with the hydrophobic groups sequestered and all the hydrophilic moieties interacting with the aqueous environment. These micelles would be more likely to interact with the inorganic components during the reaction due to the high density of carboxyl groups which could electrostatically bind to several calcium ions. This hypothesis could explain why the addition of phenylalanine to the HAp synthesis has a greater effect on the Ca/P ratio than the addition of aspartic acid.

V- Protein entrapment in hydroxyapatite:

The temperatures used in the hydrothermal syntheses of HAp were not suitable to the entrapment of protein in the inorganic network. Proteins are sensitive to heat, and most proteins undergo significant conformational changes above 80 °C. The objective of this part was to synthesize hydroxyapatite by precipitation at room temperature in order to allow the incorporation of proteins. The samples were analyzed by TEM, FTIR, XRD and BET. In order to facilitate detection lysozyme was labeled with a fluorescent probe fluorescein isothiocyanate. Complementary adsorption studies of lysozyme on various HAp samples were also performed.

V-1 Precipitation of HAp with protein entrapped

V-1-a Materials

The following materials were used: Hap synthesized from the previous reaction at 220 °C; high-purity deionized water (US Filter, Purelab Plus UV/UF); 0.1 N HCl (Aldrich); KOH (Mallinckrodt); lysozyme hen egg white (Sigma); FITC (fluorescein isothiocyanate, Aldrich); boric acid (Aldrich); ethylenediaminetetraacetic acid (Aldrich); tetrasodium salt hydrate (Aldrich); sodium borate decahydrate (Aldrich); Tris [hydroxymethyl]aminomethane hydrochloride (Mallinckrodt). The syntheses were conducted in 1000 ml Pyrex beaker.

V-1-b Preparation of the protein solution

V-1-b-i Unlabeled protein:

150 mg of lysozyme is dissolved in 100 ml of borate buffer (pH=9.2).

V-1-b-ii Labeled protein:

Hen egg lysozyme was reacted with FITC in 200 ml 0.1 M pH 9.2-borate buffer for 1 hour at room temperature in the dark. The ratio was 0.4 mole of FITC (2mg) per mole of lysozyme (150 mg) and the protein concentration was 0.75 mg/ml. The protein solution was then dialyzed against a large excess of TRIS buffer (pH=7.4) during three hours in a vigorously stirred vessel at 0 °C [16]. The buffer was then replaced and the solution was dialyzed for an additional three hours in order to remove all the unreacted FITC.

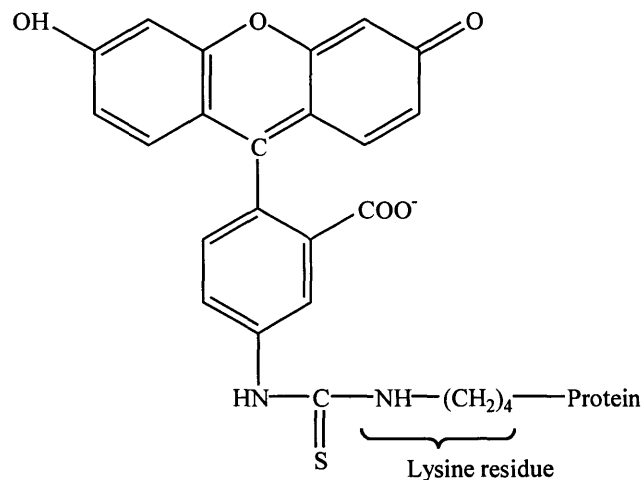


Figure V-1: FITC conjugate with ϵ -amino group of a lysine residue in a protein.

The dialysis was analyzed by UV-vis absorption spectroscopy (Beckman, DU640 spectrophotometer) to confirm that FITC was not present.

The following molar extinction coefficients were used to determine the average ratio of labels to lysozyme (L) by UV-vis absorption spectroscopy:

$$\varepsilon_{\text{lys}}^{\lambda=278}=3.206 \cdot 10^4 \text{ M}^{-1} \text{ cm}^{-1}$$

$$\varepsilon_{\text{FITC}}^{\lambda=500}=6.984 \cdot 10^4 \text{ M}^{-1} \text{ cm}^{-1}$$

$$\varepsilon_{\text{FITC}}^{\lambda=278}=1.944 \cdot 10^4 \text{ M}^{-1} \text{ cm}^{-1}$$

The labeling ratio was found to be $L=0.437 \pm 0.05$. It has previously been shown by differential scanning calorimetry analyses of labeled and unlabeled protein that the labeling procedure has little effect on the lysozyme conformation [16].

V-1-c Precipitation of HAp in the presence of protein:

HAp was synthesized by the precipitation procedure described in the previous section (I-2-b-ii) but with the addition of protein to the supersaturated solution at pH=5.

The precipitates were vacuum filtered, washed, and dried at room temperature. From the above synthesis, approximately 450 mg of HAp was obtained. The samples were characterized by XRD, FT/IR and TEM using the same instruments and sample preparation than in the first part of this work.

V-1-d Adsorption of FITC-lysozyme on precipitated HAp:

To reproduce the same conditions that for the precipitation in the presence of protein, 100 ml of protein solution were added to 900 ml of deionized water. 450 mg of

HAp previously precipitated in the absence of protein were added to the solution and the pH was raised to 8 by addition of KOH 0.5 M. The solution was left stirring overnight.

The precipitates were vacuum filtered, and dried at room temperature.

V-1-e Dissolution of HAp in EDTA buffer:

HAp can be dissolved in EDTA buffer which chelates the calcium ions breaking down the inorganic matrix. EDTA buffer is composed of 38.018 g of ethylenediaminetetraacetic acid, tetrasodium salt hydrate dissolved in 180 ml of 0.1 M HCl and 820 ml of 100 mM phosphate buffer pH=7. The pH was then adjusted to 5 by addition of HCl 0.1 M and/or KOH 0.1 M.

V-2 Results:

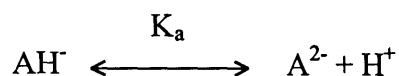
V-2-a Fluorescence Emission of FITC-lysozyme conjugates:

During the precipitation of HAp in the presence of protein, FITC-lysozyme conjugates can whether be entrapped in the inorganic network or adsorbed on the HAp surface. The objective of labeling lysozyme with a fluorescent probe is to be able to differentiate adsorbed FITC-lysozyme from intracrystalline conjugates. First, two fluorescence quenching methods of FITC-lysozyme conjugates are presented: pH quenching and methyl viologen quenching. However, none of this methods allow to conclude on the existence or not of entrapped organic material. Finally, the presence of intracrystalline lysozyme molecules will be shown by treating the HAp precipitated in the presence of labeled lysozyme with 1 wt % aqueous sodium hypochlorite in order to oxidize any surface-adsorbed proteins.

Fluorescence spectra were obtained using a Spex spectrofluorimeter at an excitation wavelength of 400 nm. Samples were contained in quartz cuvetts (12.5x12.5x45 mm). Emission spectra were scanned between 430 and 600 nm. A three milliliters solution of FITC-lysozyme solution, 0.75 mg of lysozyme per ml of solution with $L=0.437 \pm 0.05$, was titrated with 0.1 M HCl. The fluorescence intensity of the solution was monitored at $\lambda=525$ nm (maximum intensity at pH=9.2) for each pH drop.

V-2-a-i pH dependence of the conjugate:

The pH dependence of FITC-lysozyme fluorescence is presented in Figure V-2. Integrated emission spectra were directly proportional to the peak heights in all cases. Thus, the fluorescence emission intensity at each pH value is reported as the peak height normalized by the peak height obtained at pH=9.2. Although fluorescein is known to exist in at least four prototropic states with three distinct pK_a values, when it is bound to lysozyme its titration behavior is found to have a single pK_a of 6.27. The fluorescence behavior of the FITC-protein conjugate is dominated by the equilibrium between the monoanion (weakly fluorescent) and dianion (highly fluorescent) forms of fluorescein [17], represented as:



However, The FITC-lysozyme conjugate did not show a complete extinction of the fluorescence emission at low pH unlike Robeson et al. experiments. They described a

complete loss of fluorescence as the pH approached 3 [16]. Therefore the pH-dependence of the FITC probe can not be used to differentiate the extracrystalline molecules of FITC-lysozyme from the intracrystalline since there will not be a full quenching of the surface adsorbed conjugates.

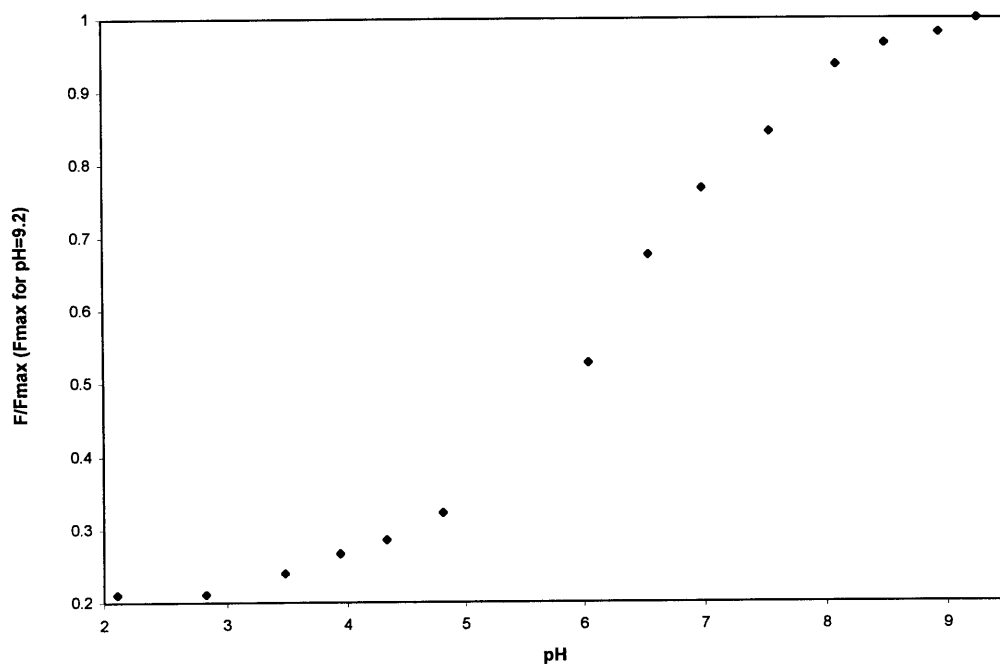


Figure V-2: pH-dependent FITC-lysozyme fluorescence intensity normalized by the fluorescence intensity at pH 9.2 at $\lambda=525$ nm.

V-2-a-ii Fluorescence quenching with Methyl Viologen:

Steady-state fluorescence was used to determine the Stern-Volmer quenching constants of methyl viologen (MV^{2+}) for FITC-lysozyme. The fluorescence intensity of the sample was measured at $\lambda=525$ nm in the absence and presence of increasing quantities of MV^{2+} using a 1 M solution. The degree of fluorescence quenching was plotted F/F_0 versus MV^{2+} concentration ($C_Q \leq 70$ mM) where F_0 is the fluorescence

intensity in the absence of MV^{2+} and F is the fluorescence intensity at a given concentration of MV^{2+} (Figure V-3):

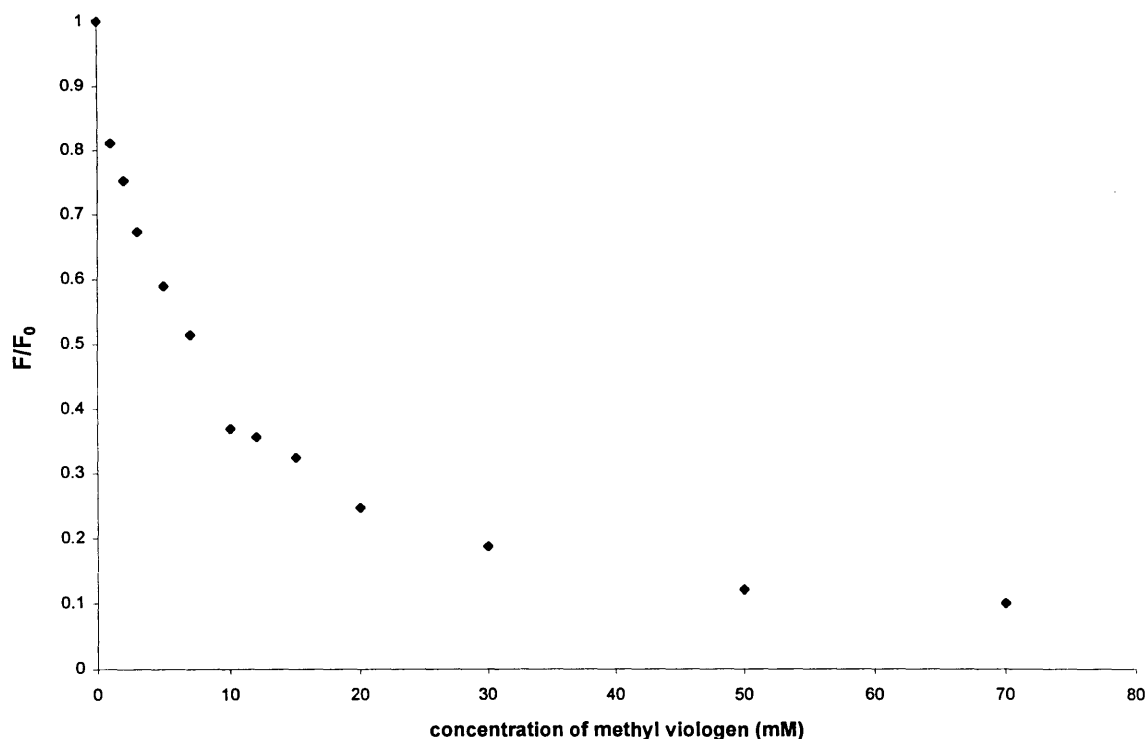


Figure V-3: Quenching of FITC fluorescence by methyl viologen at $\lambda=525$ nm.

The Stern-Volmer quenching constant K_Q was determined from the following equation which is plotted Figure V-4:

$$F_0/F=1+K_Q \cdot C_Q$$

The Stern-Volmer constants describe the quenching behavior of the quencher Q (MV^{2+}) at a given wavelength ($\lambda=525$ nm). The low value of K_Q (0.1469) shows that MV^{2+} is not an efficient quencher of the FITC-lysozyme conjugate. There still appears to be a residual fluorescence signal at high quencher concentrations ($C_Q=70$ mM) ruling out the possible use of MV^{2+} to differentiate extracrystalline and intracrystalline FITC-lysozyme by quenching the surface adsorbed conjugates.

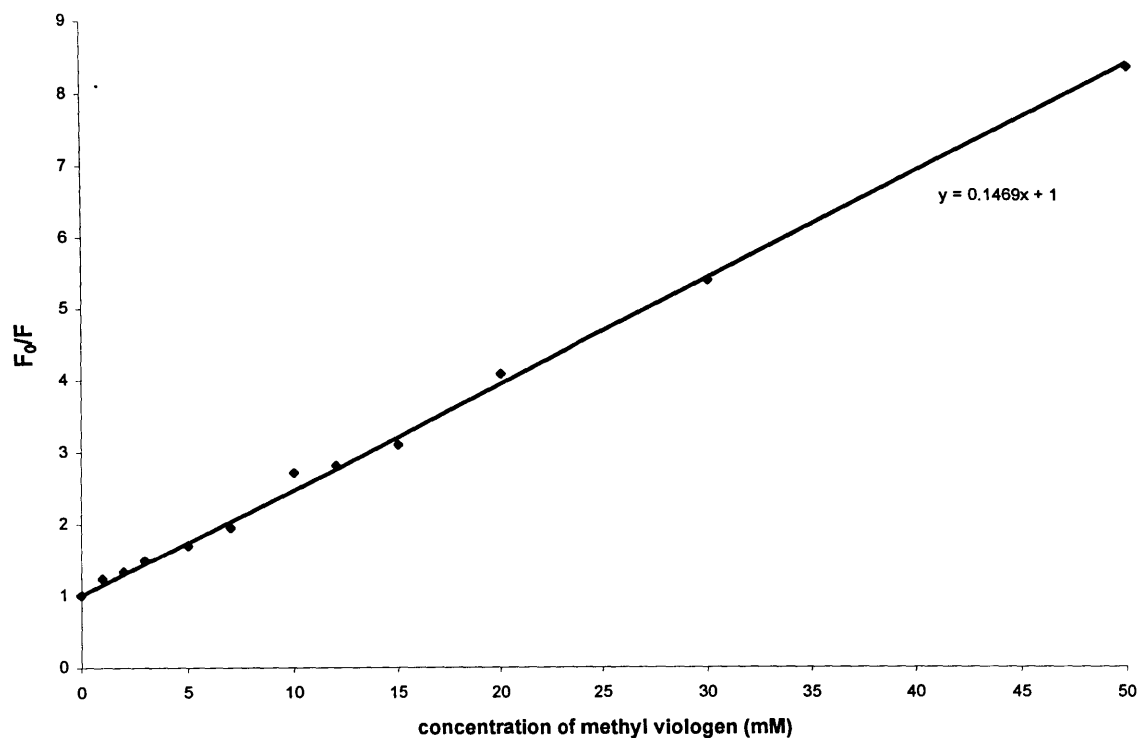


Figure V-4: Determination of the Stern-Volmer constant at $\lambda=525$ nm.

V-2-d-iii Entrapment of FITC-lysozyme:

Two sample of HAp were prepared by the precipitation method: one in the presence of FITC labeled lysozyme, and one with no added protein. The latter material was used in an adsorption experiment to determine whether FITC-lysozyme could adsorb on precipitated HAp under the conditions of the synthesis of FITC-lysozyme composite synthesized directly via precipitation.

Both samples were treated with 1% sodium hypochlorite to oxidize any surface-adsorbed proteins. The samples were suspended in borate buffer (pH 8) and their fluorescence emission intensities were monitored between $\lambda=450$ nm and $\lambda=700$ nm. The data in Figure V-7 show that, for FITC lysozyme adsorbed on the surface of the pre-

formed Hap, no fluorescence is observed which suggests that the hypochlorite treatment removed all the protein on the surface. By contrast, for HAp precipitated in the presence of FITC-lysozyme, the presence of a fluorescent signal suggests that not all the protein is removed by the hypochlorite treatment, and thus that there could be protein entrapped in the inorganic crystals.

The latter sample was dissolved in EDTA buffer. The data in Figure V-6 show that, after dissolution of the HAp matrix, a small amount of FITC lysozyme is detectable in solution.

V-2-b X-ray diffraction:

Figure V-5 shows that the peaks in the pattern of HAp precipitated in the presence or absence of FITC-lysozyme are consistent with the XRD pattern of Hap synthesized hydrothermally the hydrothermal Hap (section II-2-a). The XRD patterns of the two precipitated samples, prepared either with or without protein, are identical, and appear to be less crystalline than the Hap prepared hydrothermally

V-2-c Infrared spectrometry:

The FTIR spectra of the precipitated samples exhibit most of the characteristics of hydroxyapatite (Figure V-6), including poorly-resolved PO_4^{3-} modes at 1087 cm^{-1} (poorly resolved), 1046 cm^{-1} , 962 cm^{-1} , 605 cm^{-1} and 565 cm^{-1} , and a weak OH stretch at 3570 cm^{-1} . However, the OH librational mode at 630 cm^{-1} is absent. Broad peaks at $1370\text{-}1660\text{ cm}^{-1}$ and a band at 870 cm^{-1} were indicative of the carbonate (CO_3^{2-}) incorporated by exposure to atmospheric CO_2 (section II-2-b).

V-3 Discussion:

The precipitation technique for the synthesis of HAp was used to entrap proteins within the crystals of HAp. The XRD and FTIR spectra demonstrate that the HAp structure is unaffected by the entrapment of lysozyme, and the high degree of disorder observed is due primarily to the low temperature at which the synthesis is done. This is likely due to the low amount of protein in the solution (1×10^{-5} and 5×10^{-5} mole·L⁻¹), and thus the very low quantity that is actually entrapped within the inorganic phase. Moreover, the observation of the TEM micrographs (see Figure V-10 and V-11) indicate that there is no significant differences between the microscopic structures of the samples precipitated with or without FITC-lysozyme.

Labeling of the lysozyme molecule with a fluorescent probe (FITC) permitted detection of the presence of protein molecules. After treatment by 1% hypochloride to remove the extracrystalline proteins, fluorescence measurement spectroscopy indicated that FITC-labeled proteins were still present in the samples, which suggests that the proteins are entrapped within the inorganic network. However, the amount of lysozyme actually entrapped is very small and there is no information about the conformation or the activity of the intracrystalline proteins.

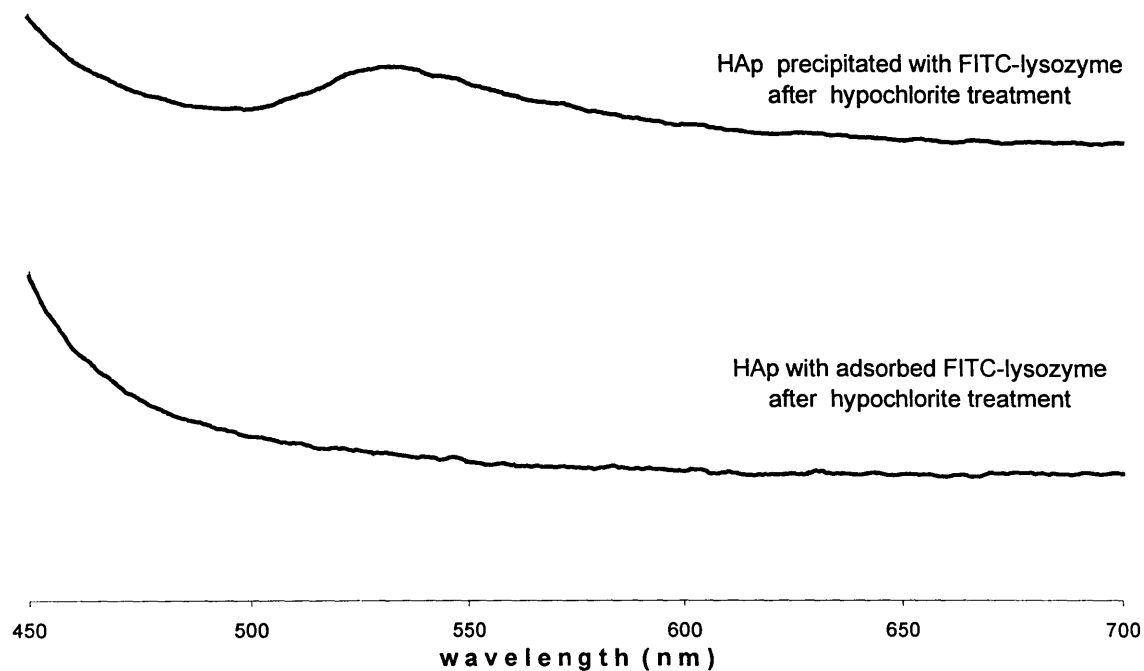


Figure V-5: Fluorescence emission of HAp precipitated with FITC lysozyme entrapped and adsorbed after treatment by 1% hypochloride.

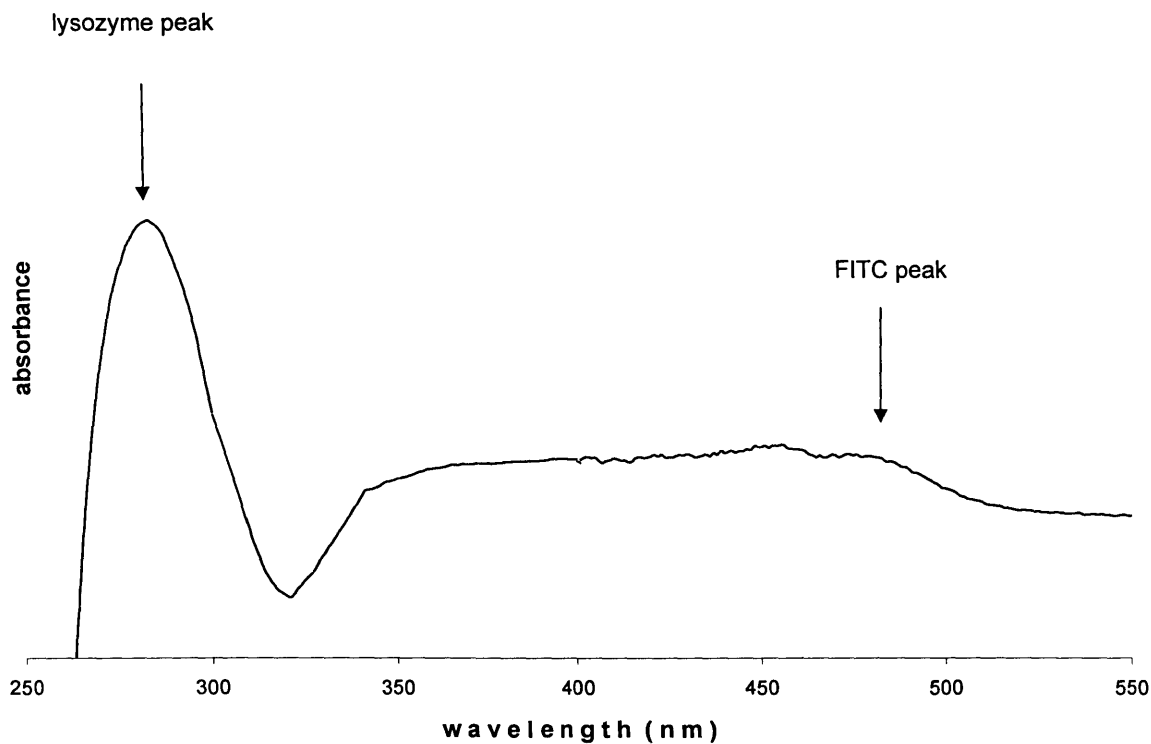


Figure V-6: UV-visible absorption spectrum of Hap/FITC-lysozyme precipitate; treated with 1% hypochloride then dissolved in EDTA buffer.

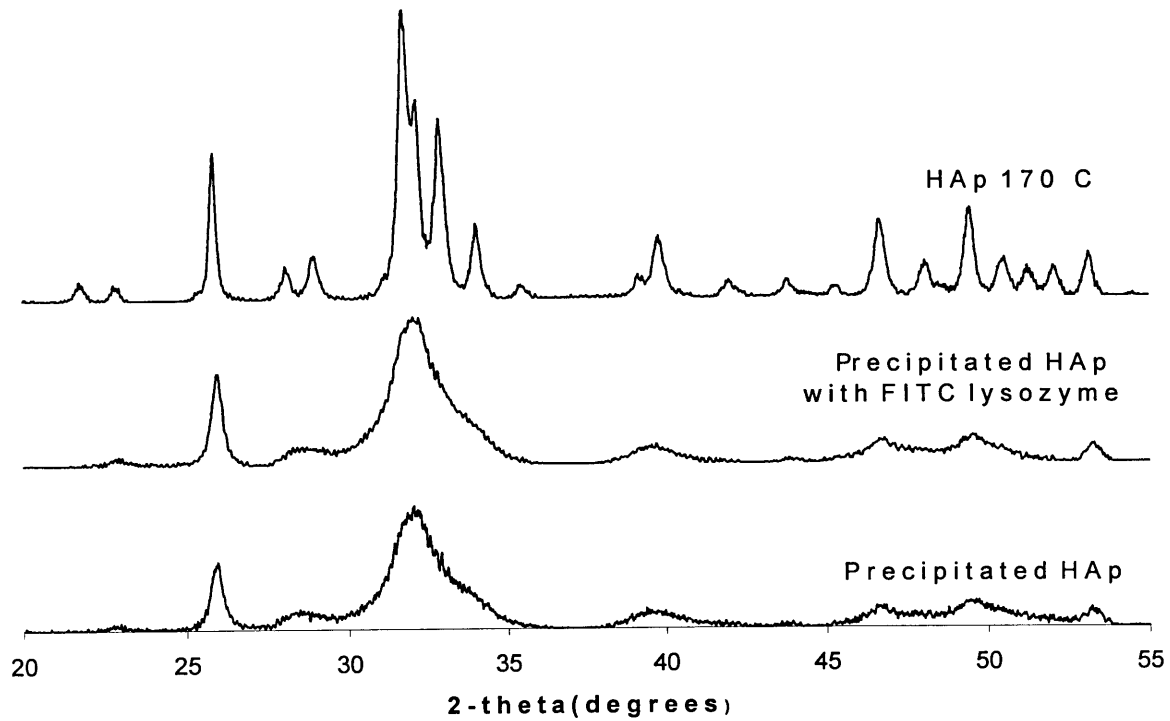


Figure V-8: Influence of lysozyme on the XRD spectrum of HAp precipitated.

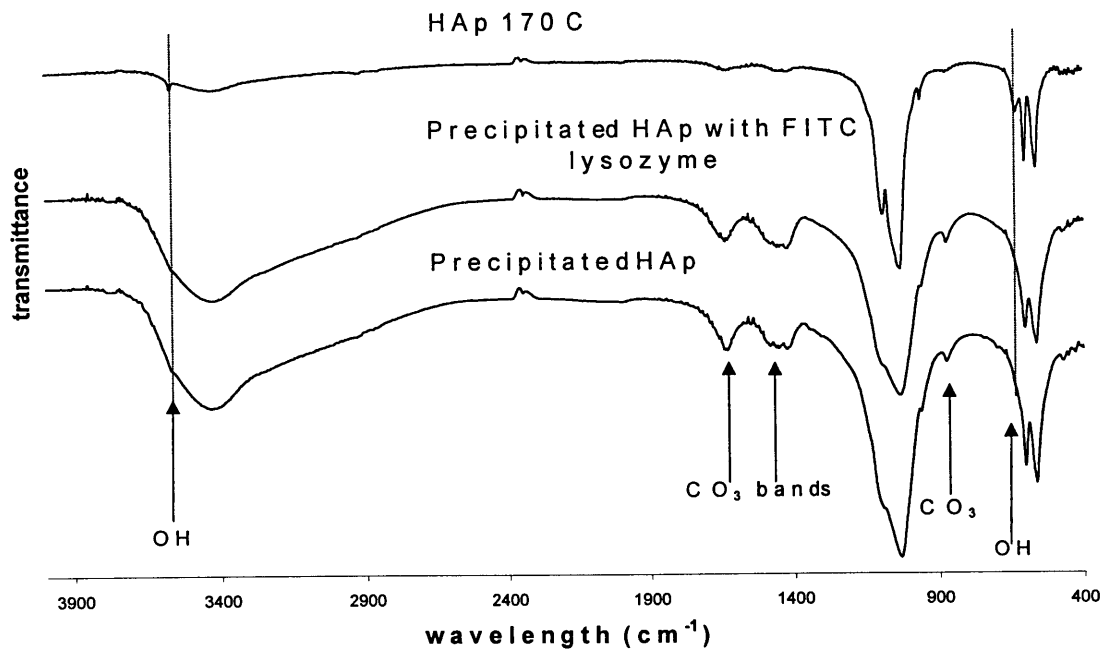


Figure V-9: Influence of lysozyme on the FTIR spectrum of HAp precipitated.

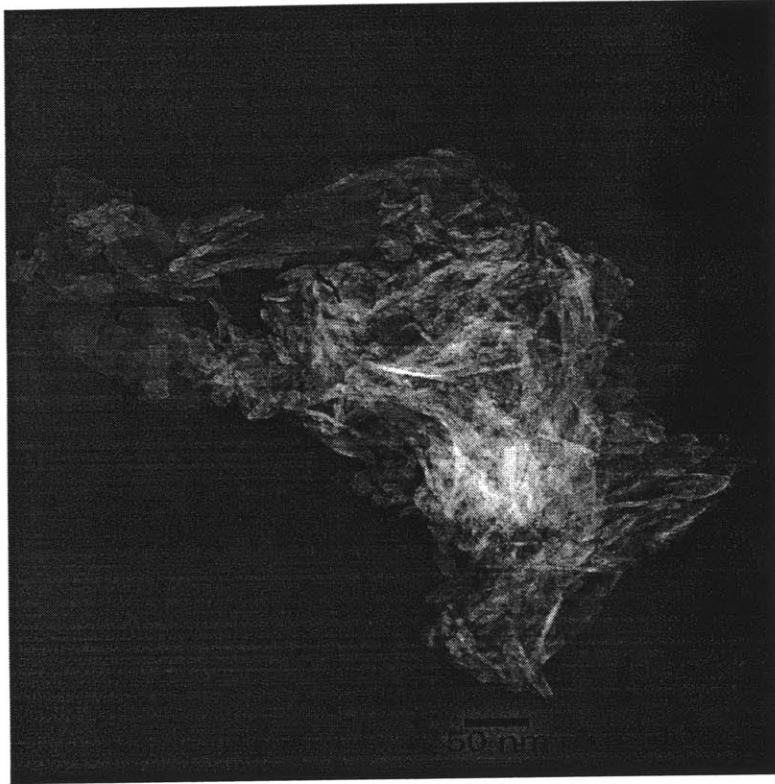


Figure V-10: Precipitated HAp.

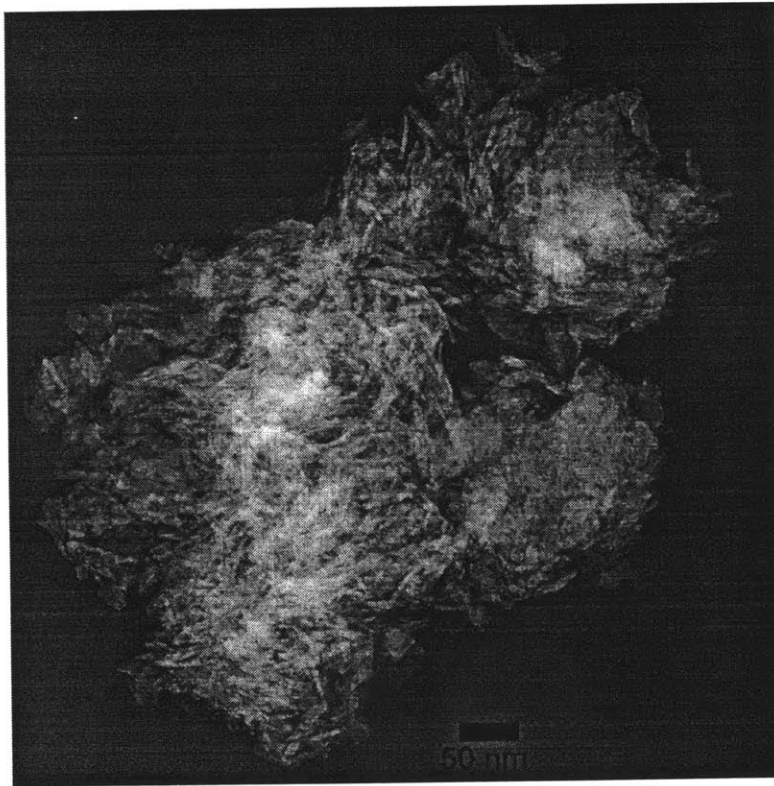


Figure V-11: Precipitated HAp with FITC labeled lysozyme.

VI- Adsorption of lysozyme on HAp:

VI-1 Interactions with hydroxyapatite [18-21]:

Proteins are long chains of amino acids. Some of these amino acids carry side chain carboxyl or amino groups which remain free and exposed to the solvent. Therefore they can dissociate in aqueous solution, resulting in COO^- and NH_3^+ ions covalently attached to the protein macromolecule. The carboxyl groups tend to ionize at pH above 4 and the amino groups below 12. At pH near pI, both NH_3^+ and COO^- groups are present and the net charge is small.

When HAp is suspended in aqueous solution, the ions on the surface are hydrated. The charge on HAp arises as a result of various dissolution and hydrolytic reactions which occur when the solid is suspended in aqueous solution [22]. The Ca/P ratio of HAp is fixed; the surface charge is function of the pH of the solution. The intrinsic point of zero charge pzc is dependent on the Ca/P ratio and the physical state. When $\text{pH} > \text{pzc}$, the ζ potential is negative and negative charge will dominate on the surface.

Only proteins in their native folded state bind effectively to HAp. That is, the ability of a protein to adsorb to hydroxyapatite is greatly diminished if its tertiary structure is disrupted from its native conformation.

The adsorption of proteins to HAp occurs through two reactions: Ca^{2+} ions can strongly bind to COO^- groups in the protein (chelate formation) and there is an electrostatic attraction between the NH_3^+ groups and the negatively charged groups of the HAp surface (PO_4^{3-} , OH^- , CO_3^{2-} ..).

VI-1-a Classification of proteins:

Proteins can be subdivided in three groups based on their isoelectric point:

1- Basic proteins, which have isoelectric points above 8. The primary eluants for these proteins are PO_4^{3-} , F^- , Cl^- , SCN^- , and ClO_4^- .

2- Neutral proteins, which have isoelectric point between 7 and 8. These proteins can be eluted with PO_4^{3-} , F^- , Cl^- but not with ClO_4^- or Ca^{2+} .

3- Acidic proteins which have isoelectric points less than 7. These proteins can be eluted with PO_4^{3-} but not with Ca^{2+} and Cl^- .

Lysozyme is a basic protein which isoelectric point is between 10.5 and 11 [18].

VI-1-b Characteristics of adsorption/elution behavior of basic proteins:

At $\text{pH} = 7.8 \pm 0.1$ which has been used in this study, lysozyme is positively charged. Therefore, the main adsorption behavior will be through electrostatic attractions between the NH_3^+ groups and the negatively-charged groups of the HAp surface.

Basic proteins are eluted by some Debye-Hückel charge screening and by some specific displacement by positive ions like Ca^{2+} or Mg^{2+} . In the solution, negatively-charged particles on the HAp surface can be considered fixed (compared to the mobility of ions and proteins). They will attract cations, creating a surplus of positive charge in its neighborhood, which reduces (or screens) its field and weakens the electrostatic force between lysozyme and the HAp surface.

VI-2 Materials and methods:

VI-2-a Materials:

Hydroxyapatite samples were prepared according to the synthesis procedures described previously.

VI-2-b Methods:

Surface charge determinations were performed using a MATEC ESA-8000 (Electrokinetic Sonic Amplitude). 2 g of solid were dispersed in 200 ml of borate buffer at pH 7.9 ± 0.1 . Single point ESA measurements were done in order to obtain the sign of the surface charge of the HAp surface for the different samples.

Adsorption experiments were carried out in 20 ml glass scintillation vials (Kimble Glass Inc, Vineland, NJ). All the volumes and weights were recorded carefully. 15 ml lysozyme solutions were prepared at concentrations of 0-0.75 mg/ml in borate buffer (0.1 M; pH 7.9 ± 0.1). A suspension of approx. 50 mg of HAp in approx. 4.5 ml of borate buffer (0.1; pH 7.9 ± 0.1) was prepared and sonicated for 15 mn. Approx. 0.5 ml of the slurry was added to the lysozyme solution. The samples were shaken gently (120 rpm) for 22 h. The samples were centrifuged during 1 h at 1500 rpm (force approx. 800·g). The lysozyme concentration in the colorless supernatant was determined from the intensity of the $\lambda = 280$ nm peak in the UV-visible absorption spectrum. The values were obtained by averaging 6 data points. In all experiments, a linear relationship between peak intensity and protein concentration was observed. The Beer-Lambert law was used to determine

amount adsorbed by monitoring the intensity of the $\lambda = 280$ nm peak before and after adsorption:

$$A = \log(I_0/I) = \epsilon \cdot c \cdot l$$

where I_0 is the intensity of the incident light, I is the intensity of the transmitted light, A is the measured absorbance, c the concentration of the absorbing species (per centimeter) and l is the path length of the light absorbing sample. The difference in absorbance before and after adsorption gives the amount of protein adsorbed on the surface. Γ (lysozyme amount in mg adsorbed per unit surface in m^2) was calculated by using the values of surface areas determined from BET. These values are consistent with the literature values commonly found for the surface areas of HAp [23-24]. Since the surface area values are obtained by nitrogen adsorption, they are probably not entirely applicable to the adsorption of a bigger molecule like lysozyme. However, it is likely that the surface accessible to the protein molecule is proportional to the BET values with the same proportionality coefficient in each case.

The surface coverage was obtained with the assumption that the lysozyme molecules adsorb side-on (Figure VI-1) and that their shape does not change upon adsorption.

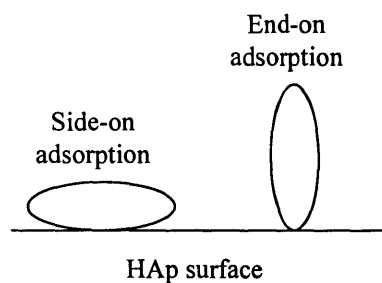


Figure VI-1: Schematic representation of side-on and end-on adsorption.

Table VI-1 presents some characteristics of lysozyme:

	Molecular weight	pI	Dimensions (Å)	Projected area (Å ²) (side-on)
Lysozyme	14,300	10.5-11	40x40x19	760

Table VI-1: Properties of lysozyme.

The surface coverage was determined by multiplying the amount in mg of lysozyme per unit area in m² (Γ) by the surface covered by 1 mg of lysozyme:

$$\theta = \Gamma \times \left(\frac{0.001 \times N_a \times 760 \times 10^{-20}}{M_{lys}} \right)$$

where N_a is the Avogadro number and M_{lys} is the molecular mass of lysozyme (14400 g·M⁻¹) .

The uncertainties of the data (error bars) were calculated by averaging the difference between the two spectra for non-absorbent wavelengths (between 300 and 500 nm). This absorbance shift is indicative of the precision of the quantitative analysis of the adsorption behavior. By the procedure previously explained, it is then possible to obtain the relative error of the different adsorption parameters calculated.

VI-3 Results and discussion:

In the pH range used for the adsorption studies (pH 8) the protein has a net positive charge. Hydroxyapatite suspended in borate buffer is also positively charged [22] as it was shown by ESA single point measurements (chapter VI-2-b). Lysozyme was selected as a test protein because it has a robust structure that is not readily denatured under the reaction conditions.

VI-3-a Adsorption isotherms:

The amounts of lysozyme adsorbed on the different samples as a function of the initial lysozyme concentration are shown in Figure VI-2. The amounts of protein adsorbed per unit surface area are shown in Figure VI-3. While there is no trend in the adsorption behavior of lysozyme at low concentration, Figure VI-2 suggests that the amount of protein adsorbed is proportional to the surface area of the mineral sample (Table VI-2).

Sample	Surface area (m ²) BET data	Amount adsorbed (mg) for a representative lysozyme concentration of approx. 52 μM	Γ (mg/m ²) for a representative lysozyme concentration of approx. 52 μM
HAp 130 °C	26	0.799	5.15
HAp 170 °C	35	0.96	4.11
HAp 220 °C	45	0.99	3.32
HAp precipitated	150-210	1.06	0.81

Table VI-2: High concentration adsorption behavior of HAp.

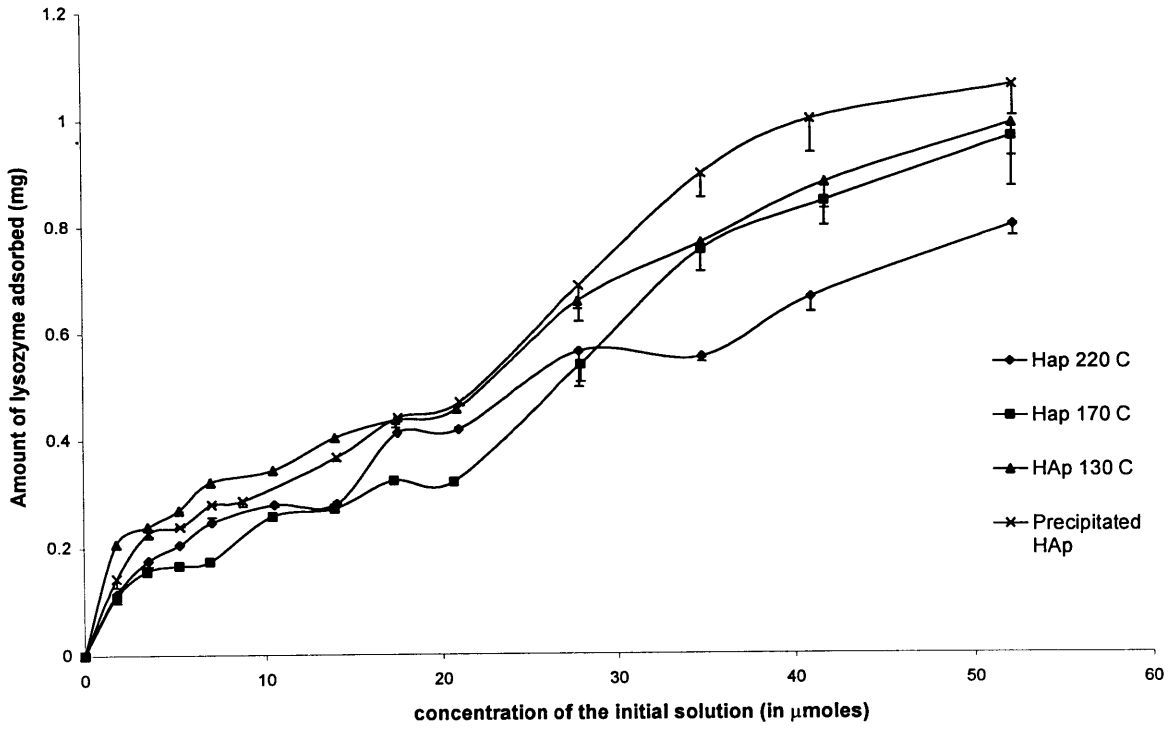


Figure VI-2: Adsorption onto Hap of lysozyme

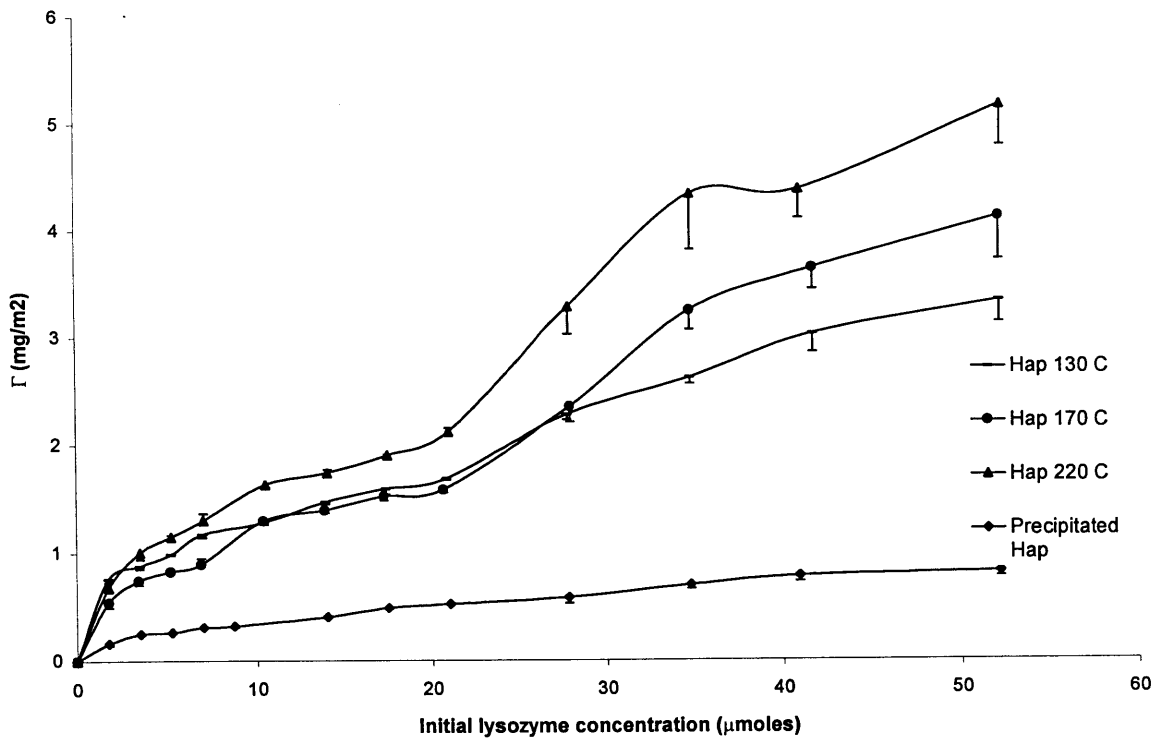


Figure VI-3: Adsorption isotherm of lysozyme (Γ as a function of concentration).

The sample with the highest surface area (precipitated HAp) has the highest amount of lysozyme adsorbed on it whereas the sample with the lowest surface area, HAp 130 °C, has the smallest amount of lysozyme adsorbed. However, at low lysozyme concentration between (0 and 30 μM) there does not appear to be any trend in the adsorption behavior. This suggests that at low surface coverage, the surface area of the sample is not a critical factor due to the number of free adsorption sites on the HAp surface.

However, the amount adsorbed per unit area (mg/m^2) follows exactly the opposite pattern. The highest Γ are obtained for the lowest surface area (see table VI-2). This suggests that the adsorption behavior of lysozyme on HAp is driven by some other factors than the surface area of the samples. The amount of lysozyme adsorbed per unit area (mg/m^2) appears to be dependent on the crystallinity and the carbonate content of the samples since HAp synthesized hydrothermally at 220 °C has the lowest content of carbonate and has the highest amount adsorbed per unit surface. The substitution of phosphate and hydroxyl by carbonate will affect the surface charge and structure (carbonate substitutions can affect the crystallographic parameters: chapter II-1) and thus modifying the surface with which lysozyme interacts. At pH 8, lysozyme and HAp have a net positive charge [22] as determined by the ESA single point measurements (VI-2-b), therefore the lysozyme molecules are electrostatically repelled from the mineral surface. A hypothesis would be that carbonate substitution increase the positive charge of the HAp surface. However, due to the size dispersion of my HAp particles that introduce an important correction factor in the evaluation of the surface charge by ESA, it was not

possible to quantify the effect of the carbonate content on the HAp surface charge. ESA data were used exclusively to determine the surface charge of Hap.

The surface coverage of HAp for the different adsorption experiments are shown in Figure VI-4. With the assumption of monolayer coverage, one common feature of adsorption to the samples that were synthesized hydrothermally is the presence of an inflection in the isotherm at approximately half-saturation, i.e., θ between 0.4 and 0.6. The isotherm shown in Figure VI-5 for HAp precipitated does not exhibit this “kink” since half-saturation has not been reached (θ between 0.2 and 0.25) due a greater surface area. This behavior has already been observed previously by Soderquist and Walton [25], in the case of the adsorption of proteins (albumin, fibrinogen) on some acidic copolymer (glutamic acid and valine) or hydrophobic polymer of ϵ -carboboxylysine and leucine. For coverage less than 0.5, adsorption is rapid and reversible and the protein molecules randomly arranged on the surface. At coverage greater than 0.5, reorganization may occur in order to allow more efficient packing and a subsequent increase in total adsorption capacity, the reorganization step gives rise to the inflection in the isotherm. Either conformational or orientational changes of lysozyme could account for the adsorption behavior. Due to the robust structure of lysozyme and the high ionic concentration of the borate buffer (0.1 M), it is unlikely that the protein would undergo any major conformational changes. The high ionic content of the borate buffer helps the protein stabilize the native conformation of lysozyme by providing negative (borate) and positive (sodium) ions. In the event of low concentration borate buffer, the protein structure is more likely to lose its native conformation by interacting with the HAp surface charges since the solution does not contain the ions providing electrostatic

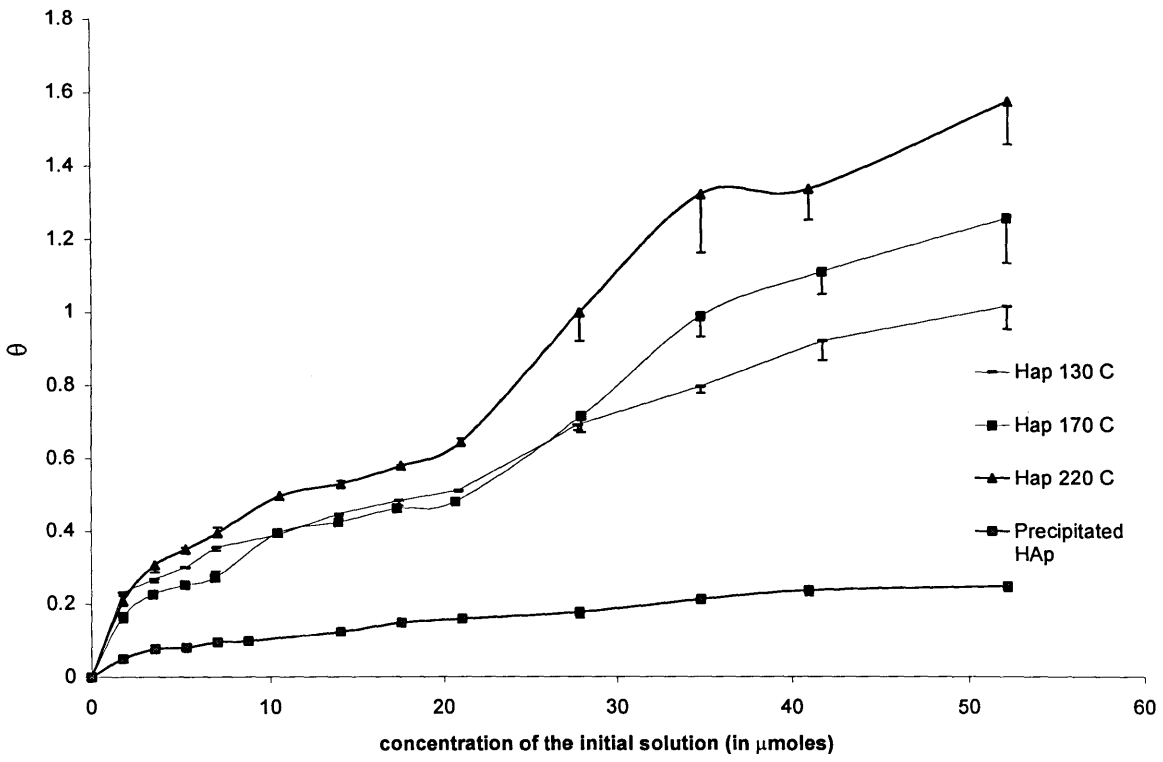


Figure VI-4: Surface coverage for lysozyme adsorption on HAp.

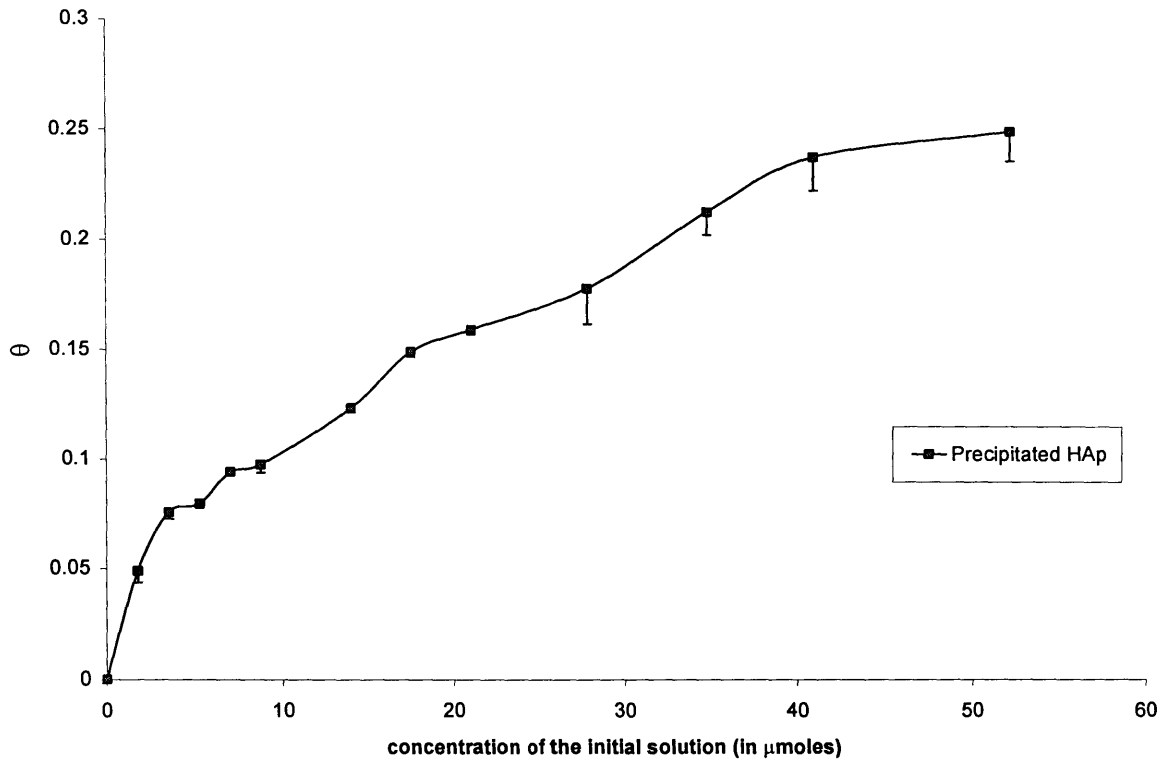


Figure VI-5: Surface coverage of the adsorption of lysozyme on HAp precipitated.

stability. Thus, the lysozyme molecules might essentially undergo orientational changes (side-on to end-on Figure VI-1). However, this reasoning only took into account the interactions between adsorbent (buffer solution) and adsorbed lysozyme molecules. At high protein concentration, the high surface coverage of the HAp surface increase the possibility of interactions between two adjacent adsorbed lysozyme molecules. Figure VI-6 schematically demonstrates the conformational changes that can occur on the lysozyme surface and introduce the notion of cooperativity.

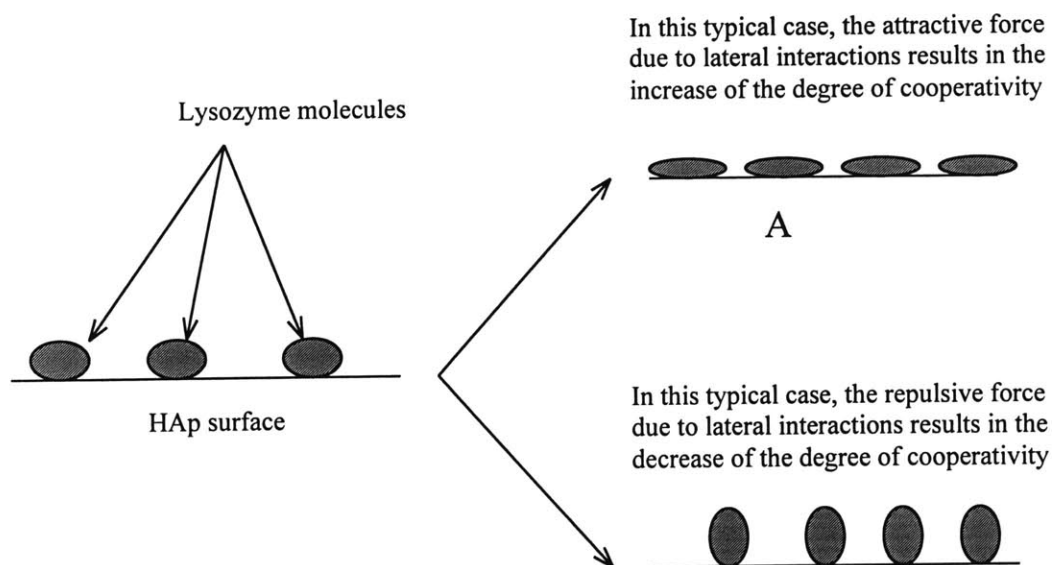


Figure VI-6: Schematic possible change of conformation due to the lateral interaction between the proteins on the surface and the interactions between protein and adsorbent.

VI-3-b Cooperativity and Hill equation:

The classical Langmuir theory for gas adsorption is often applied to quantitatively treat protein adsorption from solution. It assumes that only one molecule can be adsorbed per site (monolayer assumption), only one type of site is present (homogeneous surface), the adsorption of one molecule does not affect the adsorption energy of other molecules

(no lateral interactions or cooperativity), only one adsorbing species is present (no competitive adsorption); dilute solution, and reversible adsorption. However, the Langmuir model is inappropriate because of: (1) multiple-site binding for proteins, which often results in irreversible adsorption, (2) the heterogeneous nature of most solid surfaces, and (3) lateral and other cooperative interactions (cooperativity). Cooperativity originates from the macromolecular nature and from multiple functional groups, which usually result in interactions with several other macromolecules. It can be defined as the binding of a protein molecule to one site influencing the affinity of the other sites for the protein. Cooperativity is positive if the binding at one site increases the affinity of other sites or negative if it decreases the affinity of other sites. Hill plots are used to evaluate the cooperativity.

The formula developed by Hill [26] was first used to describe the binding between hemoglobin and oxygen. Andrade and Luo [23], used the Hill's model to describe the adsorption of proteins on HAp:

$$\theta/(1-\theta) = K \cdot [P]^n$$

$$\log \theta/(1-\theta) = \log K + n \cdot \log [P]$$

where θ is the ratio of the HAp surface covered by protein to the total surface of HAp [23], K is the Hill constant, n is the Hill coefficient which characterizes cooperativity and, $[P]$ is the bulk concentration of protein. Hill plots for HAp synthesized hydrothermally and precipitated at room temperature are presented in Figure V-7 and Figure VI-8. While this is not meant to be used as a quantitative analysis of adsorption, the Hill plots suggest useful information regarding changes in adsorption behavior.

The Hill coefficient depends on the concentration of adsorbed protein at the HAp surface. The degree of cooperativity can be considered in four states: positive ($n > 1.5$), partially positive ($1 < n < 1.5$), partially negative ($0.5 < n < 1$) and negative ($n < 0.5$).

VI-4: Discussion

The values of the Hill coefficient calculated for HAp 130 °C, HAp 170 °C, HAp 220 °C and precipitated HAp are presented in table VI-3. At coverage under 0.5, the different systems display a negative cooperativity ($n < 1$). This can be explained by the fact that both the protein and the HAp surface are positively charged under the conditions of adsorption. Because there are few negative sites on the surface to which the protein can adsorb, the adsorption of an individual lysozyme molecule decreases the number available of adsorption sites and increase the electrostatic repulsion as the next lysozyme molecule adsorb leading to a negative cooperativity

Sample	n_1 (before half coverage)	n_2 (after half coverage)
HAp 130 C	0.5291	3.9887
HAp 170 C	0.6587	15.876
HAp 220 C	0.7526	20.159
Precipitated HAp	0.1511	—

Table VI-3: Calculated Hill coefficients.

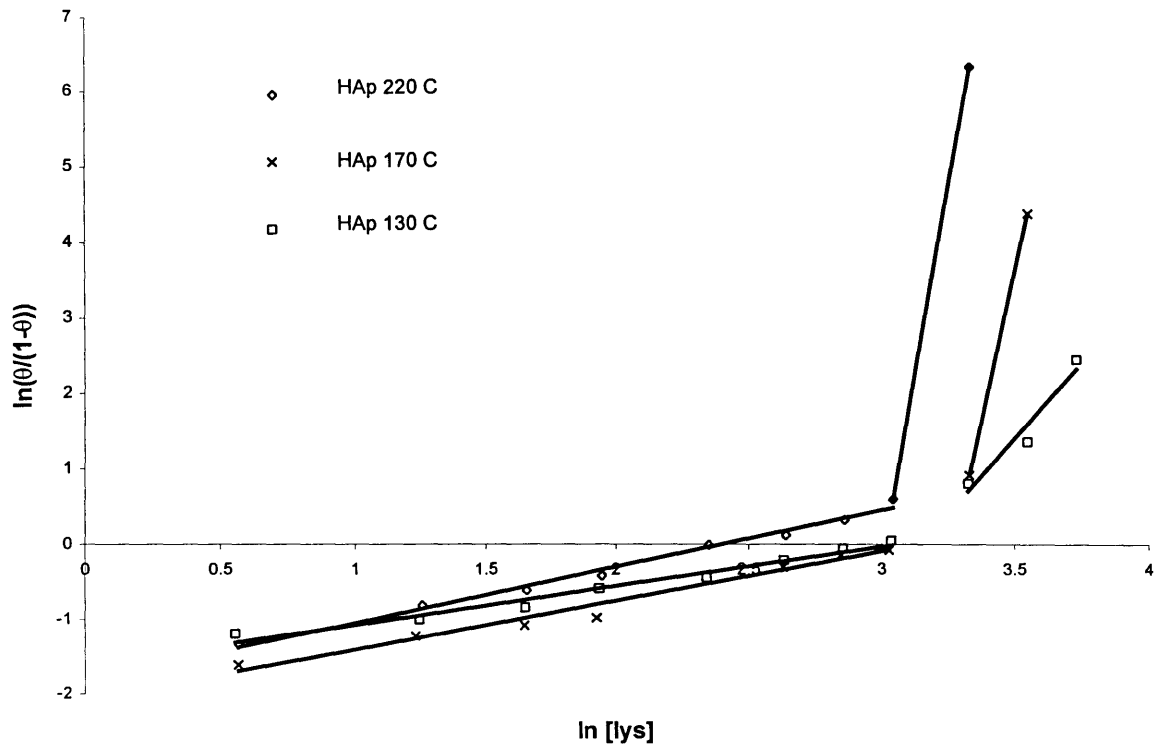


Figure VI-7: Hill plots for adsorption of lysozyme onto hydrothermally synthesized HAp samples.

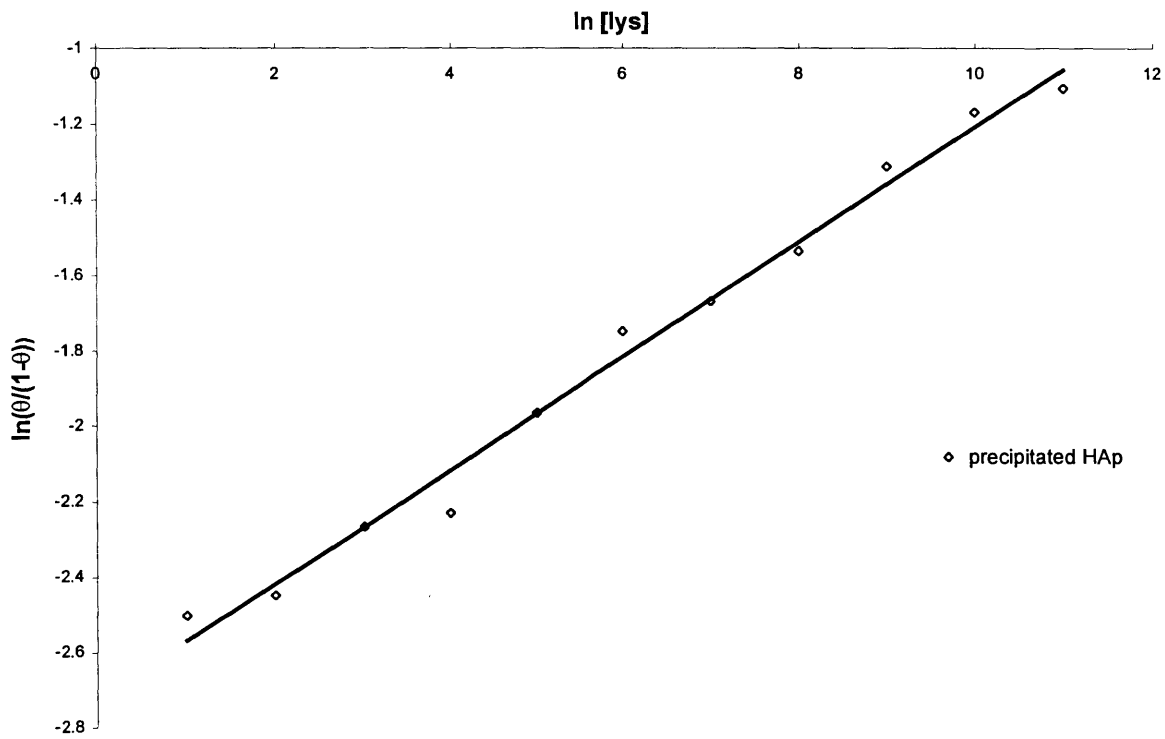


Figure VI-8: Hill plot for adsorption of lysozyme onto precipitated HAp.

However, at coverage over 0.5 the adsorption behavior changes to a positive cooperativity ($n > 1$). The modification of the adsorption behavior may be due to a conformational and/or orientational changes at the HAp interface. Figure VI-6-A shows the increase of cooperativity due to a change in conformation of the lysozyme molecule. Generally, if the lateral interaction force, due to the interaction between adsorbed lysozyme molecules and between proteins and solvent, is attractive the protein coverage on the adsorbent would be increased due to the conformational change (Figure VI-6-A), which results in the increase of the cooperativity [23].

However, lateral forces may also induce only orientational changes (side-on to end-on orientation, Figure VI-1).

Another possibility is the formation of lysozyme dimers. Sato et al. [27]-12] showed that at pH between 5 and 10, lysozyme can also be found as a dimer at room temperature and low concentration (0.2 mg/ml). These dimers could whether form in the solution and adsorb on the HAp surface or directly form on the surface which would increase the cooperativity of the adsorption behavior.

VII- Conclusion:

The initial goal of this research project was to create intracrystalline organic inclusions in hydroxyapatite. Amino acids, with a negative charge and a polar side-chain (threonine and aspartic acid), were entrapped in the HAp network by using a hydrothermal reaction at 170 ° C. Phenylalanine which was not expected to interact with the inorganic network and be incorporated because of its nonpolar side chain. An explanation would be the formation of micelles that would screen the hydrophobic R side chains and favor interactions between the hydrophilic outside and the inorganic network. Moreover, the addition of these amino acids induced the formation of some other calcium phosphate phases with lower Ca/P ratios: monetite $\text{CaPO}_3(\text{OH})$ and whitlockite (tricalcium phosphate) $\text{Ca}_3(\text{PO}_4)_2$. This suggests that the amino acids interact with the calcium ions from the inorganic network forming ionic and hydrogen bonds disturbing the stoichiometry of the solution.

Entrapment of proteins required a synthesis of HAp that could be used at room temperature. The robust protein, lysozyme, was labeled with a fluorescent probe fluorescein isothiocyanate (FITC) in order to facilitate investigation of the location of the proteins in the product. The samples precipitated with FITC-labeled lysozyme were treated with 1% dilute sodium hypochloride in order to remove surface-adsorbed protein molecules and the samples were then characterized by fluorescence spectroscopy to show the existence of intracrystalline inclusions since the entrapped molecules should not have been affected by the bleach treatment.

The last objective was to study the adsorption of lysozyme on the different Hap samples synthesized due to the importance of the bioceramic (HAp)/proteins surface

interactions in any biomaterial applications. In the hypothesis of a side-on adsorption (V-2-b) using the surface area calculated by BET, the adsorption of lysozyme on HAp can be divided into two distinct phases: first, before half coverage, a non cooperative adsorption due to the weak electrostatic repulsion between the positive surface and protein; second, after half coverage a highly cooperative adsorption that can be due to orientational or conformational changes of the lysozyme molecules. Another hypothesis to explain the high cooperativity would be the formation of lysozyme dimers.

However, many questions remain to be answered in order to understand how organic intracrystalline inclusions can be incorporated into minerals such as HAp. For example, it would be interesting to figure out the mechanism of the interactions of amino acids with the inorganic network. It is also unclear in which conformation and orientation were the lysozyme molecules entrapped in HAp. The reason behind the change of cooperativity of lysozyme adsorption on HAp could also been investigated but would require a different approach allowing a detailed study of the structure of the protein at the solid-liquid interface.

Bibliography:

1. Belcher, A.M., *et al.*, *Control of Crystal Phase Switching and Orientation by Soluble Mollusk-Shell Proteins*. *Letters to nature*, 1996. **381**: p. 56-58.
2. Lowenstam, H.A. and S. Weiner, *On biomineralization*. 1989, New York, NY 10016: Oxford University Press, Inc.
3. Addadi, L., *et al.*, *Resolution of Conglomerates by Stereoselective Modifications*. *Nature*, 1982. **296**: p. 21-26.
4. Mann, S., *Biomineralization: the hard part of Bioinorganic Chemistry!* *J. Chem. Soc. Dalton Trans.*, 1993: p. 1-9.
5. Falini, G., *et al.*, *Control of Aragonite or Calcite Polymorphism by Mollusk Shell Macromolecules*. *Science*, 1996. **271**: p. 67-69.
6. Mann, S., J. Webb, and R.J.P. Williams, *Biomineralization: Chemical and Biochemical properties*. 1989, New York, NY10010-4606: VCH publishers.
7. Simkiss, K. and K.M. Wilbur, *Biomineralization: Cell Biology and Mineral deposition*. 1989, San Diego, CA 92101: Academic Press Inc.
8. Kretsinger, R.H. and D.J. Nelson, *Coordination Chem. Rev.*, 1976. **18**: p. 29-124.
9. Weiner, S., *Phil. Trans. R. Soc. Lond.*, 1984. **304**: p. 425-434.
10. Weiner, S. and L. Hood, *Science*, 1975. **190**: p. 987-989.
11. Addadi, L. and S. Weiner, *S. Proc. Natl. Acad. Sci USA*, 1985. **82**: p. 4110-4114.
12. Bonel, G., *Contribution a l'Etude de la Carbonation des Apatites*. *Ann. Chim.*, 1972. **7**: p. 65-88.
13. LeGeros, R.Z., *Crystallographic Studies of the Carbonate Substitution in the Apatite Structure*, . 1967, New York University.
14. LeGeros, R.Z., *Apatite in Biological systems*. *Prog. Crystal Growth Charact.*, 1981. **4**: p. 1-45.
15. Sibilia, J.P., *Materials Characterization and Chemical Analysis*. Second Edition ed. 1996, New York: VCH Publishers Inc.
16. Robeson, J.L. and R.D. Tilton, *Spontaneous Reconfiguration of Adsorbed Lysozyme Layers Observed by Total Internal Reflection Fluorescence with a pH-Sensitive Fluorophore*. *Langmuir*, 1996. **12**: p. 6104-6113.
17. Ygueribide, J.E., *et al.*, *Photochem. Photobiol.*, 1994. **60**: p. 435.
18. Gorbunoff, M.J., *The Interaction of Proteins with Hydroxyapatite: I. Role of protein charge and structure*. *Analytical Biochemistry*, 1984. **136**: p. 425-432.
19. Gorbunoff, M.J., *The Interaction of Proteins with Hydroxyapatite: II. Role of acidic and Basic groups*. *Analytical biochemistry*, 1984. **136**: p. 433-439.
20. Gorbunoff, M.J., *The Interaction of Proteins with Hydroxyapatite: III. Mechanisms*. *Analytical biochemistry*, 1984. **136**: p. 440-445.
21. Radford, S.E., *et al.*, *Proteins: Structure, Function and Genetics*, 1992. **14**: p. 237-248.
22. Bell, L.C., A.M. Posner, and J.P. Quirk, *The Point of Zero Charge of Hydroxyapatite and Fluoroapatite in Aqueous Solutions*. *Journal of Colloid and Interface Science*, 1973. **42**: p. 250-261.
23. Luo, Q. and J.D. Andrade, *Cooperative Adsorption of Proteins on Hydroxyapatite*. *Journal of Colloid and Interface Science*, 1998. **200**: p. 104-113.

24. Johnsson, M., *et al.*, *Adsorption and Mineralization Effects of Citrate and Phosphocitrate on Hydroxyapatite*. *Calcif. Tissue. Int.*, 1991. **49**: p. 134-137.
25. Soderquist, M.E. and A.G. Walton, *Structural Changes in Proteins Adsorbed on Polymer Surfaces*. *J. Colloid. Interface. Sci.*, 1980. **75**: p. 386-392.
26. Hill, A.V., *Proceedings iv. J. Physiol. (London)*, 1910. **40**.
27. Sato, T., *et al.*, *Effect of Protein Aggregation on the Binding of Lysozyme to Pyrene-Labeled Polyanions*. *Langmuir*, 1998. **14**: p. 5430-5437.